

The unique allosteric property of crocodilian haemoglobin elucidated by cryo-EM

Received: 26 November 2023

Accepted: 25 June 2024

Published online: 02 August 2024



Katsuya Takahashi¹, Yongchan Lee¹, Angela Fago², Naim M. Bautista³, Jay F. Storz³, Akihiro Kawamoto⁴, Genji Kurisu⁴, Tomohiro Nishizawa¹✉ & Jeremy R. H. Tame¹✉

The principal effect controlling the oxygen affinity of vertebrate haemoglobins (Hbs) is the allosteric switch between R and T forms with relatively high and low oxygen affinity respectively. Uniquely among jawed vertebrates, crocodilians possess Hb that shows a profound drop in oxygen affinity in the presence of bicarbonate ions. This allows them to stay underwater for extended periods by consuming almost all the oxygen present in the blood-stream, as metabolism releases carbon dioxide, whose conversion to bicarbonate and hydrogen ions is catalysed by carbonic anhydrase. Despite the apparent universal utility of bicarbonate as an allosteric regulator of Hb, this property evolved only in crocodilians. We report here the molecular structures of both human and a crocodilian Hb in the deoxy and liganded states, solved by cryo-electron microscopy. We reveal the precise interactions between two bicarbonate ions and the crocodilian protein at symmetry-related sites found only in the T state. No other known effector of vertebrate Hbs binds anywhere near these sites.

For over 400 million years, haemoglobins (Hbs) from all jawed vertebrates have shared the same tetrameric organisation, with two α and two β subunits^{1,2}. These proteins generally fall into two classes, either with intrinsically low oxygen affinity when purified, or with high affinity that is reduced by binding to organic phosphates³. The human red blood cell, for example, contains 2,3-diphosphoglycerate (DPG). These heterotropic effectors are non-competitive inhibitors of oxygen binding, which the MWC allosteric model⁴ explains by their preferential binding to a low oxygen affinity T state, more constrained by inter-subunit bonds than the high affinity R state⁵. Crocodilian Hbs, however, are governed unusually strongly by carbon dioxide, and their sensitivity to chloride ions and ATP is highly variable^{6–8}. Hb from other vertebrates binds carbon dioxide more strongly on deoxygenation (the Haldane effect), but this effect is about twice as strong in crocodilian Hb as in adult human HbA, and independent of pH⁹. In the deoxy state, crocodilian Hbs bind two equivalents of bicarbonate ions per

tetramer, with a dissociation constant close to 2 mM, but the oxygenated form of the protein shows no significant bicarbonate binding². While earlier studies did not distinguish between carbon dioxide or bicarbonate ion binding, recent evidence indicates that the same amino group of crocodilian Hbs binds either carbon dioxide covalently (if unprotonated, to form a carbamino group) or bicarbonate non-covalently, if protonated^{10–12}. Bicarbonate ions, the predominant form of carbon dioxide in aqueous solution under physiological pH conditions, therefore strongly antagonise oxygen binding, increasing the oxygen tension at half-saturation (p50) of the blood by 40 mmHg and reducing the Hill cooperativity coefficient^{2,11}.

Crocodilians are descendants of a terrestrial ancestral archosaur, whereas living species such as the American alligator are ambush predators that can hide underwater for extended periods, and which kill their prey by drowning. The adaptations that led to this semi-aquatic lifestyle are still being revealed by fossils from the Upper

¹Graduate School of Medical Life Science, Yokohama City University, Suehiro 1-7-29, Yokohama 230-0045, Japan. ²Department of Biology, Aarhus University, C. F. Møllers Alle 3, Aarhus DK-8000 Aarhus C, Denmark. ³School of Biological Sciences, University of Nebraska, 1104 T St., Lincoln NE 68588-0118 NE, USA.

⁴Institute for Protein Research, Osaka University, 3-2, Yamadaoka, Suita, Osaka 565-0871, Japan. ✉e-mail: t-2438@yokohama-cu.ac.jp; jtame@yokohama-cu.ac.jp

Jurassic, when the modern crocodilian body plan appeared¹³, but the ability to use carbon dioxide to drive almost all the oxygen out of the bloodstream is clearly central to it.

In 1981, Perutz and colleagues proposed that crocodilian Hb had evolved bicarbonate binding by a very limited number of mutations relative to the DPG-binding site of human Hb, at the central cavity of the tetramer, between the N-termini of the β subunits¹⁴. This speculative model involved bicarbonate ions donating a hydrogen bond to Glu 144 of crocodilian Hb, which replaces Lys 144 of human HbA. Attempts to recreate this binding site by mutating HbA failed to produce any response to bicarbonate, and it was suggested instead by Tame that an entirely novel binding site involved a triplet of positively-charged residues (β 38–40) conserved in the C helix of crocodilian β globin¹⁵. Very unusually, crocodile Hbs also carry a tyrosine residue instead of phenylalanine at position β 41 (Fig. S1). Confirmation of this idea was achieved in 1995 by replacing five β subunit residues of human HbA, but a bicarbonate effect as strong as that found in natural proteins was only produced after a further seven mutations were introduced into the α subunits as well¹⁶. This chimeric protein, called Hb Scuba, shows very high intrinsic oxygen affinity, roughly 10 times that of normal human HbA, and much lower stability. A residue-by-residue approach to test the evolution of bicarbonate binding found that adding the Hb Scuba mutations to a reconstruction of Hb from the ancestral archosaur did not increase bicarbonate sensitivity¹². Adding ten further residues common to ancestral crocodilian and human HbA gave a protein with 59% of the full bicarbonate effect of ancestral and modern crocodilians, and 21 residues were identified that together produced the full effect¹².

Long-standing efforts to produce well-diffracting crystals of Hb Scuba have failed. Native crocodilian Hbs have also proved refractory to crystallisation¹⁷, but improvements in cryo-electron microscopy (cryo-EM) hardware and software now make it possible, although highly challenging, to solve the structures of proteins as small as Hb, which has a molecular weight of around 64 kDa. Models of oxidised (met) Hb have been determined by cryo-EM using either a Volta phase plate¹⁸, or ultraflat graphene-supported grids¹⁹. The final resolution of these maps was 3.2 Å and 3.5 Å respectively. 2.8 Å resolution was achieved with more conventional methods by Herzik and colleagues²⁰. All of these studies used commercially available lyophilised human Hb, which may have been a factor in limiting resolution. Instead, here we use conventional cryo-EM single particle analysis and fresh protein samples, stored in the liquid state under carbon monoxide to prevent oxidation.

Results

Alligator Hb (hereafter HbAM) was purified from blood taken from an American alligator (*Alligator mississippiensis*), and stored at 4 °C under carbon monoxide. The preparation of EM grids proceeded smoothly under air with the liganded protein samples, but an anaerobic chamber was required to prepare grids successfully with the deoxy protein in the presence of bicarbonate. For HbAM, the resolution limits of the carbonmonoxy, oxy, and deoxy EM maps are 2.29 Å, 2.31 Å, and 2.20 Å, respectively (Fig. 1a–c and Table 1). Equivalent datasets for human HbA achieved resolution limits of 2.27 Å, 2.24 Å, and 2.35 Å. Diatomic haem ligands were clearly visible in the maps of both HbAM and human HbA (Fig. 1d–g and Table S1), and were modelled with suitable distance restraints²¹. A water molecule is found within the haem pockets of the two deoxy models (Fig. 1h, i).

Like human HbA, HbAM has 141 residues forming seven helices in the α subunits and 146 residues forming eight helices in the β subunits (Fig. S1). The two proteins show 68% sequence identity in the α subunits, and 58% in the β subunits. The quaternary structure is strongly conserved between the two proteins, as shown by the principal allosteric contacts listed in Table S2. Helical regions are traditionally labelled from A to H²²; the loss of the D helix by α globin is very

ancient²³. Analyses of animal Hbs demonstrated decades ago that the $\alpha_1\beta_1$ and $\alpha_2\beta_2$ interfaces are relatively fixed on allosteric transition of the protein, but the interfaces between these dimers show significant differences, especially at the so-called “switch” interface between the α subunit C helix and the β subunit FG corner^{22,24–26}.

The cryo-EM model of deoxy HbAM shows an rmsd of 0.99 Å over all 574 C α atoms with the crystal structure of deoxy human HbA (PDB 2dn2)²⁷, and an rmsd of 0.42 Å with our cryo-EM deoxy human HbA model. Overlaying X-ray derived models of liganded human HbA, some of which have missing N-terminal residues, on carbonmonoxy HbAM shows a closer similarity of the R state model PDB 2dn3 (rmsd 1.15 Å over 570 C α atoms) than the R2 model PDB 1bbb²⁸ (rmsd 1.71 Å over 570 C α atoms). The cryo-EM models of oxy and carbonmonoxy human Hb show a rmsd of 0.21 Å with each other over their 566 C α atoms. Unlike HbAM, the cryo-EM models of liganded human HbA are structurally closer to the R2 form than the R structure, with rmsds of 0.58–0.60 Å and 1.44–1.46 Å, respectively. Comparison of the liganded and unliganded forms of Hb shows a concerted rotation of one $\alpha\beta$ dimer relative to the other (Fig. 2). In the case of HbAM, the rotation is 16°, with a translation of 2.4 Å. Crystal structures of R state human HbA show a similar rotation, but slightly smaller translation of 1.3 Å, compared to deoxy HbA²⁷. Salt bridges found in T-state human HbA are conserved in HbAM, including the bond formed within each β subunit by Asp 94 (in HbA) or Glu 94 (in HbAM) and His 146, consistent with both proteins having a similar chloride-independent Bohr effect (Fig. S2).

The bicarbonate binding site is deeply buried at the “flexible joint” region of the $\alpha_1\beta_2$ interface formed by the α FG corner and the β C helix (Fig. 3), a location not associated with other heterotropic effectors, which is probably why Perutz discounted it. The hydrogen bonds formed by the ligand are shown in Fig. S3. Almost all of these direct contacts are formed with a single β subunit, including the unique crocodilian residues Lys β 38(C4) and Tyr β 41(C7). CO₂, as well as bicarbonate ions, can bind to the same site of crocodilian Hbs¹³, and the side-chain of Lys β 38 is clearly well-placed to bind either ligand, by covalent or hydrogen bond, respectively. The α subunit accepts a single hydrogen bond through the carbonyl oxygen of Arg 92, requiring the ligand to donate a hydrogen bond and accounting for the bicarbonate specificity. Introduction of the bulky lysine side-chain in place of Thr β 38 displaces the β C helix, including the key allosteric residues Trp β 37(C3), and Asn β 102 (Fig. 3f). Lys β 38 and the conserved Arg β 40 sandwich the bicarbonate ion (Fig. 3g, h), suggesting side-chain repulsion in the absence of bicarbonate ions, but Arg β 40 is relatively flexible. A number of novel interactions are seen in the deoxy HbAM model however which appear to counter the destabilisation caused by the Lys-Arg-Arg triplet. Tyr β 41 forms a hydrogen bond with the main-chain nitrogen of Asp β 99. Arg β 39 replaces glutamate in human HbA, and points in a direction away from the bicarbonate, to form hydrogen bonds with the carbonyl oxygen atoms of four different residues, Leu β 32, Pro β 36, Met β 48, and Cys β 49 (Fig. 3i). Two valine residues of human HbA in this region (β 33 and β 54) are replaced with isoleucine, while Pro 51 of human HbA is replaced with alanine in HbAM. There is no obvious role for the Gly β 29→Ser mutation in Hb Scuba, but the Leu β 31→Met mutation is probably required to hold the Lys β 38 side-chain in place.

The seven α subunit mutations of Hb Scuba cluster around the CE corner, with Tyr α 36 of HbAM (replacing Phe α 36 of human HbA) in contact with both Leu α 100 and His α 103 of the same subunit (Fig. 4a). Komiyama et al. found that without the Leu α 100→Phe mutation, Hb Scuba lost not only the bicarbonate effect but all cooperative oxygen binding, an effect that remained entirely unexplained¹⁶. In the deoxy HbAM model it can be seen that the side-chains of Tyr α 36 and Phe α 100 lie parallel, but in human HbA Leu α 100 pushes Phe α 36 slightly towards the β_1 subunit. This movement would disrupt hydrogen bonds made by Gln β 131, as would a side-chain larger

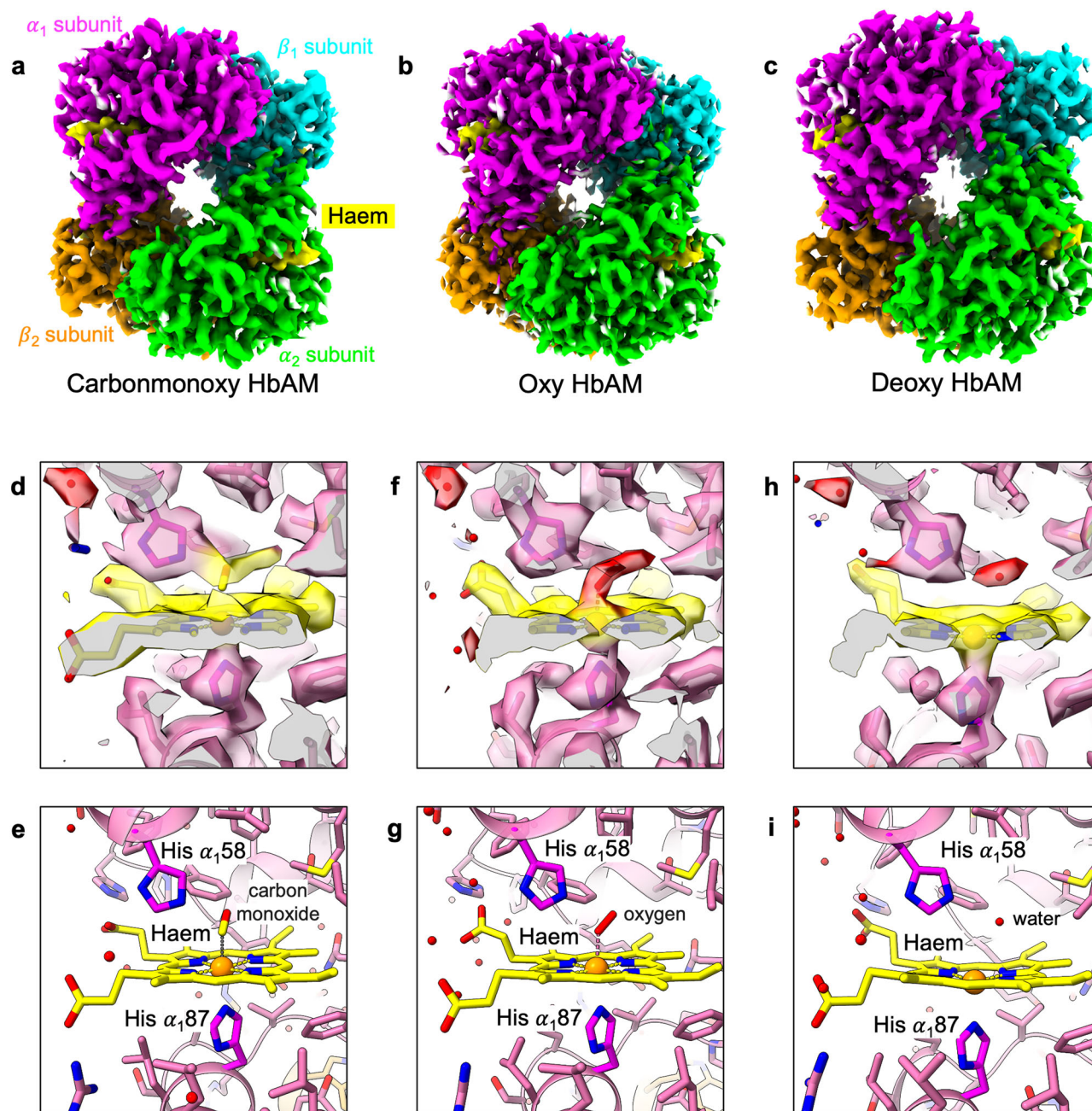


Fig. 1 | Cryo-EM density maps. **a** carbonmonoxy, **b** oxy, and **c** deoxy HbAM, shown with different colours for each subunit. α_1 : magenta, α_2 : lime, β_1 : cyan, β_2 : orange, haem: yellow. Cryo-EM density around the haem in the α_1 subunit of carbonmonoxy

HbAM (**d**, **e**), oxy-HbAM (**f**, **g**), and deoxy HbAM (**h**, **i**). The carbon atoms of the haem and ligands are shown in yellow. The characteristic doming of the deoxy haem is clearly visible in **h**.

than alanine at α_{35} (Fig. 4). In the deoxy HbAM structure, Arg β_{135} hydrogen bonds to the carbonyl oxygen of Ala α_{35} , another interaction that would be prevented by the presence of Leu α_{100} pressing against Tyr α_{36} . Even though Arg β_{135} is only found in Hbs of crocodiles and birds (alanine is generally conserved at this position) it remained entirely overlooked until modelling studies in 2020⁸. The missing Ala→Arg mutation at β_{135} appears to be at least partly responsible for the instability and high oxygen affinity of Hb Scuba, although allosteric switching to the carbonmonoxy form brings the C-terminal carboxyl group of His β_{2146} within 5 Å of the Arg β_{135} guanidino group, weakening its interaction with Ala α_{35} (Fig. 4c). Crocodilian Hbs strengthen the $\alpha_1\beta_1$ interface by replacing Ala α_{120} with glutamate, forming additional van der Waals contacts with Ala β_{51} .

The carbonmonoxy form of HbAM shows many of the expected features, with the conserved residues of the allosteric core forming the same interactions as in human HbA (Table S2). In switching to the R state, relative motions of the two $\alpha\beta$ dimers place the carboxyl group of Asp α_{194} close enough to form hydrogen bonds with the side-chains of Tyr β_{241} and Asn β_{2102} , roughly where bicarbonate sits in the deoxy T state (Fig. 3j). This tyrosine residue therefore provides an extra hydrogen bond to stabilise the R state. In all other vertebrate Hbs the β subunit C7 residue is phenylalanine, probably due to its role in holding the haem in place^{29,30}. α globin has tyrosine at the equivalent position (Tyr α_{42}), which forms an important T state hydrogen bond with Asp β_{299} (Table S2B)³¹. Tyrosine residues in close proximity to haem groups are liable to single electron reduction in the presence of peroxides, giving long-lived tyrosine radicals that can cause oxidative

Table 1 | Data collection and refinement statistics for all models

PDB EMDB	CO-HbAM 8WIX 37571	O ₂ -HbAM 8WJY 37572	Deoxy HbAM 8WIZ 37573	CO-HbA 8WJO 37574	O ₂ -HbA 8WJ1 37575	Deoxy HbA 8WJ2 37576
Data collection/processing						
Magnification	165,000	165,000	165,000	165,000	165,000	165,000
Voltage (kV)	300	300	300	300	300	300
Electron exposure (e ⁻ /Å ²)	60.0	60.0/58.4	58.4	58.4	58.4	58.4
Defocus range (μm)	-0.4 to -1.2	-0.4 to -1.2	-0.4 to -1.2	-0.4 to -1.2	-0.4 to -1.2	-0.4 to -1.2
No. of frames	54	54	54	55	55	54/56
Pixel size (Å)	0.51	0.51	0.51	0.51	0.51	0.51
Micrographs	5775	16,056	12,001	8994	9002	16,579
Initial particles	7,296,950	10,003,848	6,675,397	4,939,556	4,542,816	8,682,020
Final particles	751,964	372,582	316,544	504,650	550,843	460,786
Symmetry imposed	C2	C2	C2	C2	C2	C2
Map resolution (Å)	2.29	2.31	2.20	2.24	2.27	2.35
FSC threshold	0.143	0.143	0.143	0.143	0.143	0.143
Map sharpening B factor (Å ²)	-85.5	-78.1	-85.7	-82.7	-88.2	-70.3
Refinement						
Initial model used (PDB code)	-	-	-	2dn1	2dn1	2dn2
Model resolution (Å)	2.3	2.3	2.2	2.2	2.3	2.3
FSC threshold	0.5	0.5	0.5	0.5	0.5	0.5
Model composition						
Non-hydrogen atoms	4980	5162	5102	4790	4732	4948
Protein residues	574	574	574	566	566	574
Ligands	8	8	6	8	8	4
B factors (Å ²)						
Protein	59.2	48.0	47.8	55.3	59.3	52.9
Ligand	47.5	34.1	35.2	41.9	46.0	39.0
R.m.s. deviations						
Bond lengths (Å)	0.0142	0.0131	0.0143	0.0140	0.0143	0.0148
Bond angles (°)	1.80	1.79	1.87	1.84	1.85	2.03
Validation						
MolProbity score	2.26	2.31	2.48	2.33	2.33	2.25
Clashscore	5.87	7.26	9.60	8.18	7.97	6.62
Rotamer outliers (%)	9.58	11.67	12.08	14.54	14.98	10.82
Ramachandran plot						
Favored (%)	96.82	97.53	97.17	98.57	98.57	97.53
Allowed (%)	2.83	2.47	2.83	1.43	1.08	2.12
Disallowed (%)	0.35	0.00	0.00	0.00	0.36	0.35

damage. On the other hand, mutating Phe β41 of HbA to tyrosine provides an extra route for electrons from reductants such as ascorbate to oxidised haem, and such mutations have been explored as means to reduce the toxicity of artificial Hb-based oxygen carriers³². Natural selection has apparently firmly chosen Phe C7 for β globin to reduce oxidative damage while demanding Tyr C7 for α globin to stabilize the T state. All diving species face heightened challenges of oxidative damage³³, which may explain the relatively high prevalence of cysteine and histidine residues in crocodilian Hbs. Four histidine residues are common to crocodilian Hbs that are not found in human HbA (Fig. S1); all of them are found at the protein surface, but away from inter-subunit contacts. His α67 and His α113 replace threonine and leucine, respectively, in human HbA. In crocodilian Hbs, residue α68 is either aspartic or glutamic acid, but the structural models offer no convincing evidence of any functional interaction with His α67. His α113 (also found in some bird Hbs) forms a hydrogen bond with Tyr α24 of the same subunit in both deoxy and liganded models, which presumably stabilises the protein but provides little Bohr effect. His β6

and His β56 are uniquely crocodilian residues, replacing glutamate and glycine residues, respectively, not only in human HbA but also in bird Hbs. Both of these histidines are solvent-exposed, providing extra buffering capacity but no additional intramolecular interactions. (β6 is the site of the Glu→Val mutation of sickle-cell Hb.) Individual species may have histidine residues not found generally among crocodilians, for example, His β52 of HbAM or His β136 of the caiman, which are also solvent-exposed, especially His β52, which sits near His β56. It is interesting to speculate that Tyr β41 first arose to accelerate the reduction of oxidized β subunits and was then co-opted as a binding site for bicarbonate ions. Human HbA carrying the mutation Phe β41→Tyr is stable but shows low oxygen affinity due to a more stable T state, possibly due to a hydrogen bond between Tyr β41 and the carbonyl of His β197³⁴.

Discussion

The solution of alligator Hb using cryo-electron microscopy solves several issues regarding Hb structure and evolution. Firstly the models

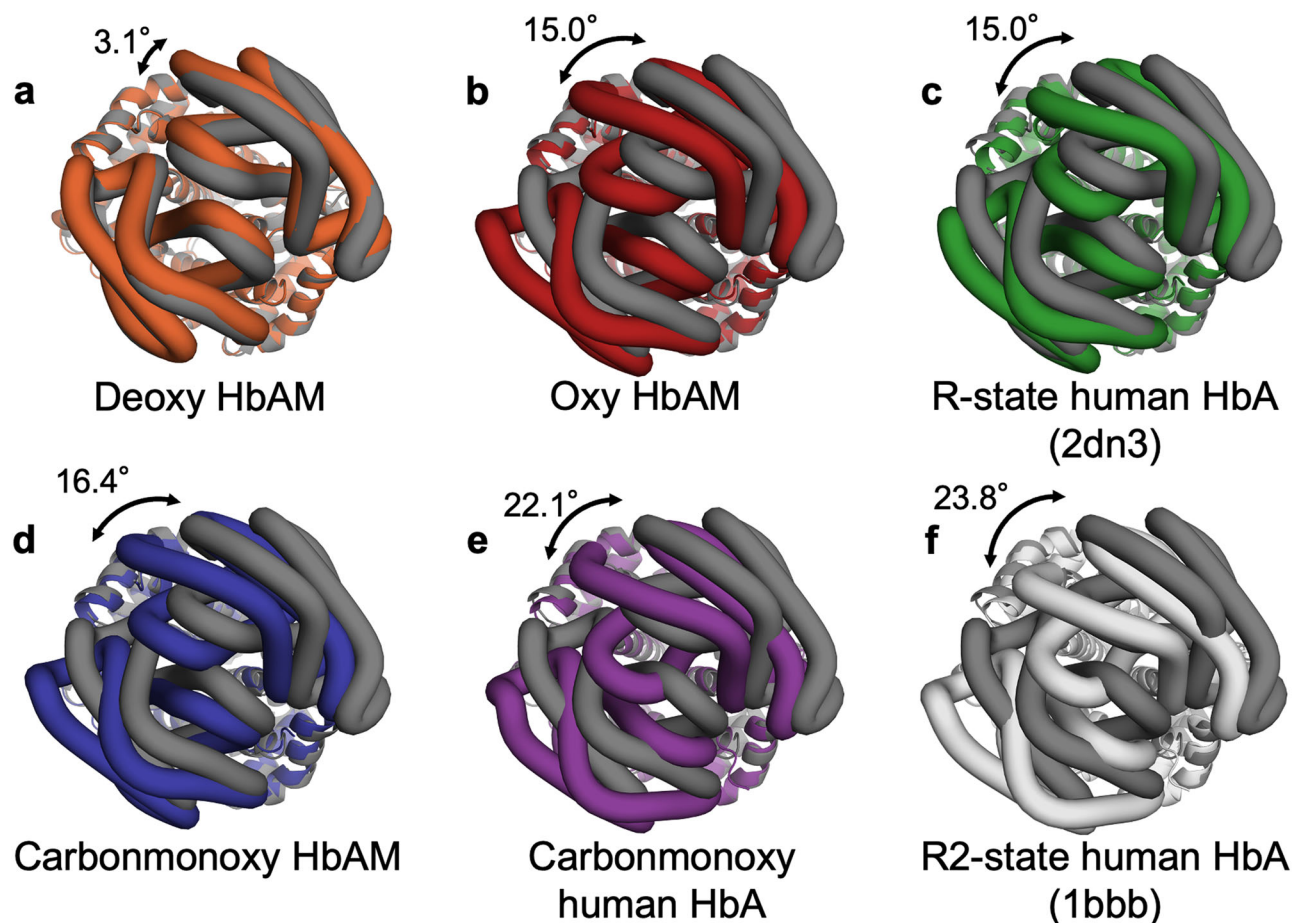


Fig. 2 | Dimer-dimer rotation angles. The $\alpha_1\beta_1$ dimers of different Hb models (shown as ribbons) were first superposed on those of the crystallographic model of deoxy human HbA (PDB 2dn2), and then the $\alpha_2\beta_2$ dimers (shown as tubes) were overlaid. The rotation angle of the second least-squares fit is indicated. The deoxy

human HbA model is shown in dark grey. **a** deoxy HbAM, orange. **b** oxy-HbAM, red. **c** crystal model of R-state carbonmonoxy human HbA (PDB 2dn3), green. **d** carbonmonoxy HbAM, blue. **e** carbonmonoxy human HbA, purple. **f** crystal model of R2-state carbonmonoxy human HbA (PDB 1bbb), white.

corroborate the X-ray crystallographic structures of human HbA, particularly in the liganded form²⁷. Considerable debate arose with the suggestion that the R-state structures of liganded Hb were artefacts arising from the high ionic strength used in crystallisation³⁵. The models here support the view that the R2 structural models represent a corner of the volume of conformational space occupied by oxy- or carbonmonoxy-Hb, and that the thermodynamic R-state is well represented by crystallographic models such as PDB 2dn1^{27,36,37}. Secondly, the structures of alligator Hb reported here, determined by a different analytical technique, underline the conservation of the allosteric mechanism of Hb over hundreds of millions of years of evolution. Some decades ago, Perutz suggested that most of the amino acid differences between vertebrate Hbs are neutral or nearly so, and that adaptive mechanisms have evolved through a few key replacements³⁸. This idea certainly fits the very low heat of oxygenation of Hb from woolly mammoths, the first protein resurrected from an extinct animal^{39,40}. Mammoths evolved from equatorial ancestors, but quickly adapted a Hb with thermal properties like those of modern polar species through a single principal mutation⁴¹. Some bird species also provide examples where single α or β subunit mutations yield the higher oxygen affinity required for high-altitude flight^{42–45}. Perutz was unable though to explain the extreme pH sensitivity of many fish Hbs, which appears to have been acquired and lost many times, by a variety of mutations affecting either the α or β subunits^{46–49}. Diving animals such as penguins are able to exploit their body oxygen stores very effectively by regulating Hb with organic phosphates and pH⁵⁰, but the

bicarbonate effect of crocodilian Hb is completely unique. Although the same mechanism could function perfectly well in other vertebrates, apparently only the lifestyle of crocodiles gave them sufficient benefit to evolve it; not only does the bicarbonate effect permit extended diving³¹, but it may play an important role in unloading oxygen from the blood during the post-prandial “alkaline tide” caused by HCl secretion sufficient to acidify the stomach enough to digest bone⁵². Experimental testing of resurrected ancestral Hbs revealed that the gain of bicarbonate sensitivity and the concomitant loss of ATP-sensitivity occurred in the line of descent leading from the ancestor of birds and crocodilians in the mid-Triassic to the common ancestor of modern crocodiles (~80 million years ago)¹². Ontology may recapitulate this evolutionary process, since the American alligator produces embryonic (Hb I) and adult (Hb II) isoforms with the same α chain, but with β subunits that share only 59% sequence identity⁵³. Hb I lacks all the β subunit residues associated with bicarbonate binding; it has high oxygen affinity and also strong sensitivity to ATP, which may help developing embryos survive hypoxic conditions in the nest⁵⁴.

Our HbAM models suggest that the creation of the bicarbonate binding site disturbs key residues responsible for the delicate balance between the R and T states of the protein, as reflected by the high oxygen affinity and instability of Hb Scuba. Only through a number of mutations is this balance restored. Overall the allosteric controls of Hb appear more fragile than its structure. Changing Thr β 38→Lys does not prevent cooperative oxygen binding, but apparently conservative mutations such as Phe α 100→Leu eliminate the bicarbonate effect.

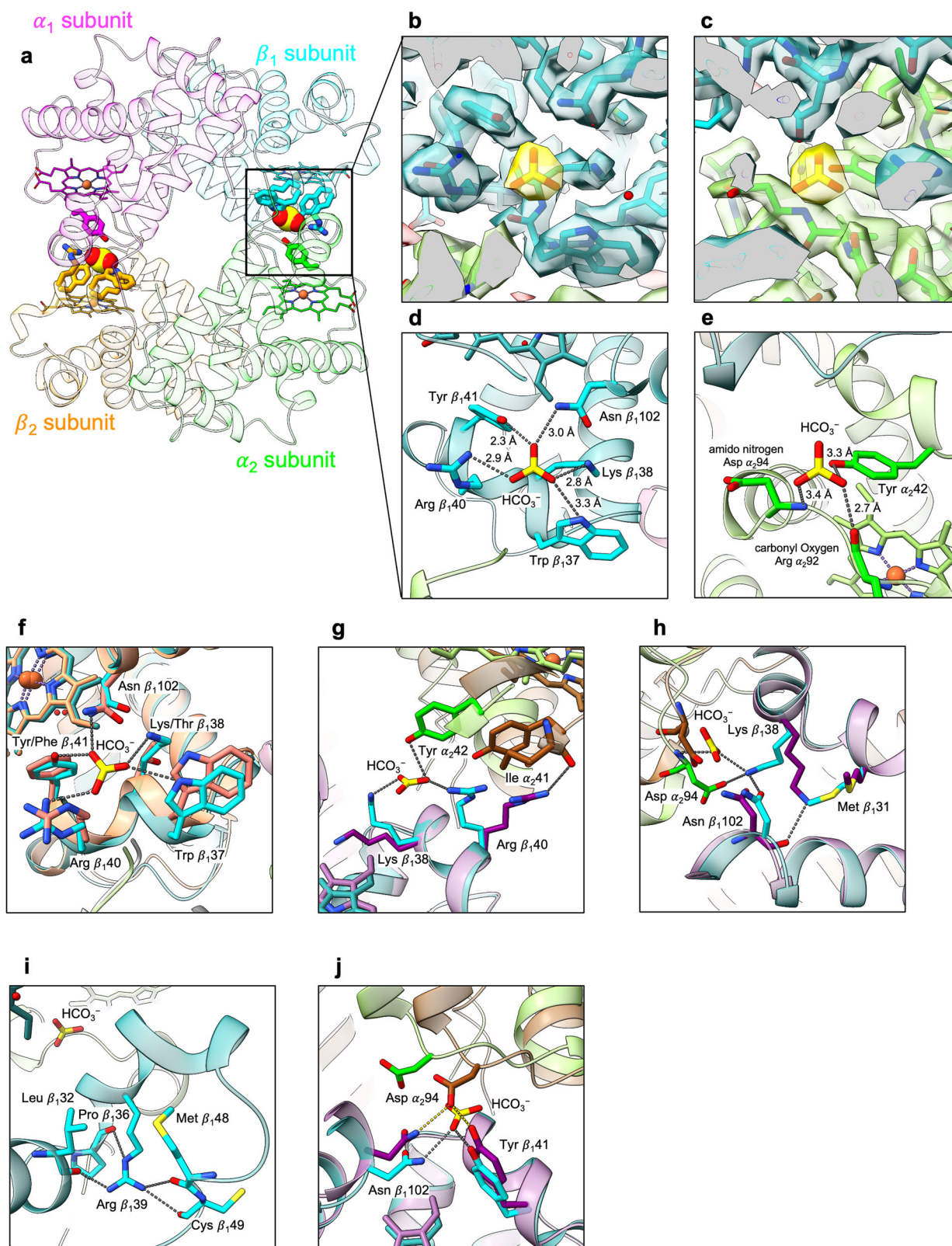


Fig. 3 | The bicarbonate ion binding site. **a** Symmetry-related bicarbonate ions are shown (as CPK models) in the deoxy HbAM tetramer, and side-chains bonding to them are shown as sticks. The carbon atoms of the α_1 subunit are shown in magenta, the β_1 subunit in cyan, the α_2 subunit in lime, and the β_2 subunit in orange. **b, c** Cryo-EM density around the bicarbonate ion and (**d, e**) the bonding interactions. The hydrogen bonds between the bicarbonate ion and side-chains are shown as grey dotted lines (with distances). **f** An overlay of deoxy HbAM and human HbA at the bicarbonate ion binding site. For deoxy human HbA, the carbon atoms of the β_1

subunit are coloured salmon, and the α_2 subunit is shown in white. **g** $\alpha_1\beta_1$ overlay of deoxy HbAM and carbonmonoxy HbAM at the bicarbonate ion binding site, showing relative displacements of Lys β_1 38 and Arg β_1 40. For carbonmonoxy HbAM, the carbon atoms of the β_1 subunit are shown in purple, and those of the α_2 subunit are shown in brown. **h** Another view of the overlay in **g**, showing Met β_1 33. **i** Interactions formed by Arg β_1 39, which points away from the bicarbonate ion. **j** A different view of the overlay in **g**, showing Asp α_2 94 and Tyr β_1 41.

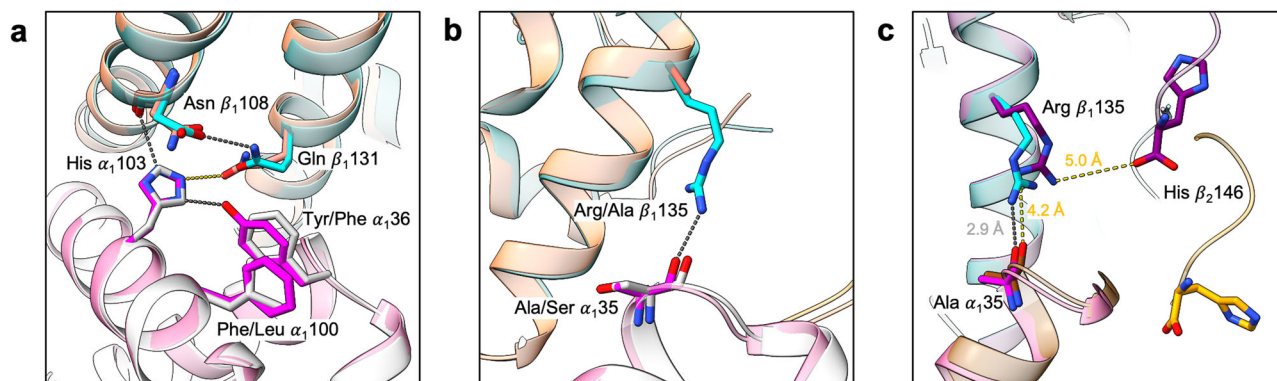


Fig. 4 | Interactions at the $\alpha_1\beta_1$ subunit interface. **a** An overlay of deoxy HbAM and human HbA around His $\alpha_1,103$. The carbon atoms of the α_1 and β_1 subunits of HbAM are shown in magenta and cyan, respectively, and those of the α_1 and β_1 subunits of human HbA are shown in white and salmon. **b** the BC corner of the α_1 subunit and the H helix of the β_1 subunit. The hydrogen bond formed by Arg $\beta_1,135$

and Ala $\alpha_1,35$ in deoxy HbAM is shown. **c** The α_1 BC corner, β_1 H helix, and the C terminus of β_2 subunit of deoxy and carbonmonoxy HbAM. The carbon atoms of the α and β subunits of carbonmonoxy HbAM are shown in brown and purple, respectively. Hydrogen bonds formed by Arg $\beta_1,135$ are shown as dotted lines, either silver (in deoxy HbAM) or gold (in carbonmonoxy HbAM).

Further work will be required to understand the stability and utility of intermediate Hbs on the evolutionary pathway that led to this unique allosteric control mechanism, but the models described here will hopefully be of immense value in the search for clinically useful Hb-based blood substitutes⁵⁵. The normal levels of bicarbonate ions in both arterial and venous human blood exceed 20 mM⁵⁶, more than ten times the bicarbonate binding constant of deoxy crocodilian Hb². Recently there have been a number of clinical trials to evaluate globin gene therapy for patients with thalassemias or sickle-cell disease⁵⁷, and two treatments received FDA approval in late 2023 (<https://www.fda.gov/news-events/press-announcements/fda-approves-first-gene-therapies-treat-patients-sickle-cell-disease>). For patients with some conditions, such as limited lung function, it may be that normal human HbA can be improved upon by borrowing functionality such as that currently unique to crocodilians.

Methods

Ethical statement

Human hemoglobin was purified by Prof. Tsuneshige of Hosei University, Japan, using standard protocols and blood freshly drawn from a human volunteer, from whom written informed consent was obtained in accordance with Hosei University Ethical Regulations for Research Involving Human Subjects (Regulation #1141). The methodology was approved by the relevant committee. Whole alligator blood used for this study was obtained by Prof. Dane Crossley of The University of North Texas from nine female adult alligators that were allocated to independent research projects. After euthanasia, a protocol for blood collection was carried out following the Institutional Animal Care Guidelines at The University of North Texas (UNT IACUC #20009). Blood was carried out with the express knowledge and permission of the relevant board at UNT.

Human HbA sample preparation. HbA was purified by Prof. Tsuneshige of Hosei University, Japan, using standard protocols and blood freshly drawn from a human volunteer. The washed red cells were bubbled with carbon monoxide before lysis, and the purified protein was shipped to Yokohama at 4 °C under carbon monoxide in stoppered tubes. Carbonmonoxy-HbA was diluted to 5.3 mg/mL with PBS (phosphate-buffered saline) to prepare EM samples. Oxy-HbA was obtained from carbonmonoxy-HbA by passing wet oxygen gas (99.5%) over the protein sample in a round-bottomed flask on ice. The sample was rotated under illumination from a table lamp, until the visible absorbance spectrum indicated oxygenation was complete. Oxy-HbA was finally diluted to 7.0 mg/mL with PBS. 3 μ L drops of the liganded

Hb were applied to grids (Quantifoil Cu/Rh R1.2/L3 carbon holey 300 mesh), which were glow-discharged in advance, and blotted for 3 s with a blot force of 10 at 6 °C and 100% humidity with using Vitrobot (Mark IV, Thermo Fisher), and then was plunge-frozen into liquid ethane.

We failed to prepare suitable deoxy HbA grids under air. In this method, a 3 μ L drop of HbA solution was applied to the grid directly after 20 mM fresh sodium dithionite was added to Oxy-HbA (7.0 mg/mL). The grid was blotted and frozen as described above. Despite changes to the absorbance spectrum measured by Nanodrop (Thermo Fisher), which showed an absorbance peak at 550 nm, the initial 3D map (reconstructed from about 30k particles) had the same structure as R-state HbA, suggesting the protein reoxygenated during the vitrification. Deoxy HbA grids were therefore prepared with a Vitrobot installed in an anaerobic chamber, with an oxygen concentration of ~10–20 ppm. Fresh 0.2% (w/v) of dithionite was added to oxy-HbA in the anaerobic chamber, giving a final concentration of 5.5 mg/mL. 2 mM IHP (inositol hexaphosphate) was also added to stabilize the T-state structure. The UV-visible spectrum of the sample was measured before it was applied to the grids and plunge-frozen in liquid ethane. The grids were glow-discharged before being brought into the anaerobic chamber.

HbAM sample preparation. Whole blood used for this study was obtained from nine adult alligators that were allocated to research projects in which euthanasia was an endpoint. After the euthanasia protocol was performed following the Institutional Animal Care Guidelines at The University of North Texas (UNT IACUC), 5 mL of blood was collected in heparinized syringes by direct puncture of the ventricle and then immediately stored at –80 °C until further use. Frozen blood was thawed on ice, centrifuged for 5 min, 4000 $\times g$ at 4 °C, and supernatant plasma was discarded. The red blood cells were washed 3–5 times with ice-cold 0.9% NaCl containing 0.5 mM EDTA, before being lysed by 1:5 dilution in chloride-free 10 mM HEPES pH 7.6, 0.5 mM EDTA, and incubated on ice for 45 min. The hemolysate was then centrifuged at 4 °C (12,000 $\times g$, 20 min) to remove cell debris. To remove small molecular weight molecules, including allosteric effectors of Hb, the hemolysate was then stripped by passing it through a PD-10 SephadexTM G-25 M desalting column (GE Healthcare) previously equilibrated with 10 mM HEPES pH 7.6, 0.5 mM EDTA.

HbAM was purified by ion exchange chromatography using a Hitrap Q XL column (Cytiva, Uppsala) equilibrated with 20 mM HEPES pH 7.6, 0.5 mM EDTA, and then eluted with a 0–0.1 M NaCl linear gradient, at a flow rate of 0.5 ml/min, at room temperature.

Absorbance was monitored at 415 nm and 280 nm to identify haem-containing proteins. The adult Hb fraction was concentrated by centrifugation (11,000 × *g*, 10 min), passed again through a PD-10 column, and dialyzed against 10 mM HEPES pH 7.4, 0.5 mM EDTA to remove NaCl. After dialysis, the sample was equilibrated with CO, flash-frozen in liquid nitrogen, and stored at −80 °C until further analysis.

CO-bound HbAM was diluted to a final concentration of 6.5 mg/mL with TN buffer (20 mM Tris and 100 mM NaCl pH 8.0), containing 10 mM of DTT (dithiothreitol). 3 µL of the sample was applied onto the grids (Quantifoil Cu R1.2/1.3 carbon holey 300 mesh), which were glow-discharged at 10 mA for 50 s in advance. The grids were blotted for 3 s with a blot force of 10, and plunge-frozen in liquid ethane with a Vitrobot (Mark IV, Thermo Fisher) at 6 °C and 100% humidity under air. DTT was added to the solution to prevent disulfide bonds and consequent aggregation. Oxy-HbAM was prepared from CO-bound HbAM as described above for human HbA. The UV-Vis spectrum was monitored to confirm that oxygen had completely replaced carbon monoxide. Immediately after sample preparation, oxy-HbAM was diluted to a final concentration of 7.0 mg/mL with DTT-contained TN buffer applied onto the grids and plunge-frozen in the same way as above. Deoxy HbAM EM grid samples were prepared inside an anaerobic chamber, in which the oxygen concentration was kept at 10–20 ppm. Oxy-HbAM was diluted to 5.5 mg/mL with TN buffer containing 10 mM DTT, 10 mM sodium bicarbonate, and 0.2% (w/v) fresh sodium dithionite. Absorbance at 550–570 nm was monitored to confirm the removal of oxygen before a 3 µL drop of protein was applied to the grid and plunge-frozen by Vitrobot inside the anaerobic chamber.

Data collection. All cryo-EM data were collected in RIKEN Yokohama, using 300 kV acceleration voltage, with a Titan Krios G4 (Thermo Fisher) equipped with a K3 detector (Gatan) in counting mode with correlative double sampling (CDS), using automated EPU software (ThermoFisher). Images were acquired at a ×160,000 magnification with a pixel size of 0.51 Å. Movies were collected with 54–56 frames using a range of −0.4 to −1.2 µm defocus with two to three shots per hole. The exposure time was 2.0 s, and the exposure dose was 7.6 e/pix/s; the total exposure was 58.4 e/Å². In some datasets, the exposure dose was 7.8 e/pix/s, and the total exposure was 60.0 e/Å². We collected 5775 micrographs for carboxy-HbAM, 9378 micrographs for oxy-HbA, 12,001 micrographs for deoxy HbAM, 8994 micrographs for carboxy HbA, 9002 micrographs for oxy-HbA, and 16,579 micrographs for deoxy HbA.

Data processing. All the datasets were processed using CryoSPARC⁵⁸, beginning with motion correction and contrast transfer function (CTF) estimation. Particles were picked automatically using Blob Picker job, extracted from the micrographs with a 256-pixel box, and Fourier cropped to 128 pixels. 2D classification was performed, and Hb-shaped 2D class averages were manually selected to build initial volumes. Three classes of ab initio models were generated, and several bad volumes were used in heterogeneous refinement as decoy to draw particles that are not clearly Hb-shaped. For carbonmonooxy-HbA and oxy-HbA, a prototype 3.9 Å resolution map of HbAM, built from about 49k particles, was used as a reference volume. For deoxy HbA, carbonmonooxy HbAM and deoxy HbAM, a high-resolution map of oxy-HbA was used as a reference volume. For oxy-HbAM, a high-resolution intermediate map of carboxy-HbAM was used as a reference volume. For all datasets, several rounds of heterogeneous refinement were performed, and the particles from the best classes were re-extracted with a 512-pixel box size and Fourier cropped to 256 pixels. Several rounds of refinement were then performed with a homogeneous set of particles, and the final maps were obtained from non-uniform refinement with C2 symmetry and optimized defocus and CTF parameters. The final HbAM maps (Figs. S5–7) were obtained with resolution of: carbonmonooxy, 2.29 Å (from 751,964 final particles), oxy, 2.31 Å

(from 372,582 final particles), deoxy, 2.20 Å (from 316,544 final particles). The final human HbA maps (Figs. S8–10) were obtained with resolution of: carbonmonooxy, 2.24 Å (from 504,650 final particles), oxy, 2.27 Å (from 550,843 final particles), deoxy, 2.35 Å (from 460,786 final particles). The overall resolution of the final maps was determined by the gold-standard Fourier shell correlation (FSC).

Model building. The HbAM models were built from an AlphaFold2⁵⁹ predicted model, and each subunit of the models was fitted to the relevant map using ChimeraX⁶⁰. The oxy and carbonmonooxy human HbA models were built from the R-state crystal structure (PDB 2dn1), and the deoxy human HbA model was built from the T-state crystal structure (PDB 2dn2) using Coot⁶¹. Model restraints were determined using ISOLDE⁶, and refinement was performed with Servcat⁶². Manual adjustments were carried out with Coot. The data collection, refinement parameters, and model statistics are summarized in Table 1.

Modelling bicarbonate ion in deoxy HbAM. Early steps of the refinement of deoxy HbAM were performed with C1 symmetry. After the map resolution improved beyond 3 Å, extra density was observed at two symmetry-related positions at the α₁β₂ and α₂β₁ subunit interfaces. A water molecule was placed in the middle of this density at each position, and model refinement was performed with Servcat⁶³, which yielded positive Fo-Fc density (as shown in Fig. S11), where a bicarbonate ion was finally modelled. The final cycles of non-uniform refinement were performed with C2 symmetry applied to the model, which improved the resolution.

Deoxy human HbA 3D classification. IHP (inositol hexaphosphate) was added to stabilize deoxy human HbA before vitrification under anaerobic conditions. After several rounds of heterogeneous refinement and non-uniform refinement with C2 symmetry, a 2.35 Å resolution deoxy human HbA map was obtained from about 460k particles. A flat and transverse region of density was observed between the N-terminal regions of the β subunits, where IHP is known to bind. Non-uniform refinement was performed with C1 symmetry, which gave a density map suggesting the phosphate groups could interact with positively-charged amino acid side-chains lining the pocket, but the map was too blurry to show this clearly. To obtain a better map of the phosphate binding site, 3D classification was performed to classify 460k particles into eight classes with a mask around the IHP map. Two major classes were obtained: 169k particles of liganded HbA in class 0 and 134k particles of unliganded HbA in class 1. Each map was locally refined with the same mask, to give a map at 2.59 Å resolution of IHP-liganded deoxy HbA and a separate map at 2.66 Å resolution of IHP-free deoxy HbA (Fig. S12a–c). For the liganded model, IHP was fitted to the map using Coot. IHP sits between Val β1, His β2, Lys β82, and His β143 of both β subunits, apparently without a single strongly preferred conformation. Compared to the crystal structure of deoxy human HbA (2dn2), the two N-terminal residues move towards IHP, and the side-chains of Lys β82 move towards the central cavity to avoid steric hindrance with IHP (Fig. S12d). Our results are broadly in line with previous crystallographic models of deoxy Hb bound to 2,3-diphosphoglycerate (Fig. S12e)^{64,65}.

Reporting summary

Further information on research design is available in the Nature Portfolio Reporting Summary linked to this article.

Data availability

The data that support this study are available from the corresponding authors upon request. The final models have been deposited in the Protein Data Bank (PDB). The cryo-EM density maps, half maps, and masks have been deposited in the Electron Microscopy Data Bank (EMDB), and the cryo-EM raw images have been deposited in the

Electron Microscopy Public Image Archive (EMPIAR). Accession codes are as follows: alligator haemoglobin in carbonmonoxy form (8WIX, EMD-37571, EMPIAR-11988), alligator haemoglobin in oxy form (8WIY, EMD-37572, EMPIAR-11989), alligator haemoglobin in deoxy form (8WIZ, EMD-37573, EMPIAR-11990), human haemoglobin in carbonmonoxy form (8WJO, EMD-37574, EMPIAR-11991), human haemoglobin in oxy form (8WJI, EMD-37575, EMPIAR-11992), human haemoglobin in deoxy form (8WJ2, EMD-37576, EMPIAR-11993).

References

- Gell, D. A. Structure and function of haemoglobins. *Blood Cells Mol. Dis.* **70**, 13–42 (2018).
- Brunori, M. & Miele, A. E. Modulation of allosteric control and evolution of hemoglobin. *Biomolecules* **13**, 572 (2023).
- Perutz, M. F. & Imai, K. Regulation of oxygen affinity of mammalian haemoglobins. *J. Mol. Biol.* **136**, 183–191 (1980).
- Monod, J., Wyman, J. & Changeux, J. P. On the nature of allosteric transitions: a plausible model. *J. Mol. Biol.* **12**, 88–118 (1965).
- Miele, A. E., Bellelli, A. & Brunori, M. Hemoglobin allostery: new views on old players. *J. Mol. Biol.* **425**, 1515–1526 (2013).
- Bauer, C. et al. Analysis of bicarbonate binding to crocodilian hemoglobin. *J. Biol. Chem.* **256**, 8429–8435 (1981).
- Bauer, C. & Jelkmann, W. Carbon dioxide governs the oxygen affinity of crocodile blood. *Nature* **269**, 825–827 (1977).
- Fago, A. et al. Structure and function of crocodilian hemoglobins and allosteric regulation by chloride, ATP, and CO₂. *Am. J. Physiol. Regul. Integr. Comp. Physiol.* **318**, R657–R667 (2020).
- Jensen, F. B., Wang, T., Jones, D. R. & Brahm, J. Carbon dioxide transport in alligator blood and its erythrocyte permeability to anions and water. *Am. J. Physiol.* **274**, R661–R671 (1998).
- Natarajan, C. et al. Effect of NH₂-terminal acetylation on the oxygenation properties of vertebrate haemoglobin. *Biochem. J.* **477**, 3839–3850 (2020).
- Bautista, N. M. et al. New insights into the allosteric effects of CO₂ and bicarbonate on crocodilian hemoglobin. *J. Exp. Biol.* **224**, jeb242615 (2021).
- Natarajan, C. et al. Evolution and molecular basis of a novel allosteric property of crocodilian hemoglobin. *Curr. Biol.* **33**, 98–108 (2023).
- Yoshida, J. et al. A new goniopholidid from the Upper Jurassic Morrison Formation, USA: novel insight into aquatic adaptation toward modern crocodylians. *R. Soc. Open Sci.* **8**, 210320 (2021).
- Perutz, M. F. et al. Allosteric regulation of crocodilian haemoglobin. *Nature* **291**, 682–684 (1981).
- Tame, J. R. H. The role of the distal residues of α globin. Ph.D. thesis, Cambridge University (1989).
- Komiyama, N. H., Miyazaki, G., Tame, J. & Nagai, K. Transplanting a unique allosteric effect from crocodile into human haemoglobin. *Nature* **373**, 244–246 (1995).
- Jandaruang, J. et al. Purification, characterization, and crystallization of *Crocodylus siamensis* hemoglobin. *Protein J.* **33**, 377–385 (2014).
- Khoshouei, M., Danev, R., Plitzko, J. M. & Baumeister, W. Revisiting the structure of hemoglobin and myoglobin with cryo-electron microscopy. *J. Mol. Biol.* **429**, 2611–2618 (2017).
- Zheng, L. et al. Uniform thin ice on ultraflat graphene for high-resolution cryo-EM. *Nat. Methods* **20**, 123–130 (2023).
- Herzik, M. A., Wu, M. & Lander, G. C. High-resolution structure determination of sub-100 kDa complexes using conventional cryo-EM. *Nat. Commun.* **10**, 1032 (2019).
- Torrens, F. A comparative study of O₂, CO and CN binding to heme IX protein models. *Molecules* **9**, 632–649 (2004).
- Baldwin, J. & Chothia, C. Haemoglobin: the structural changes related to ligand binding and its allosteric mechanism. *J. Mol. Biol.* **129**, 175–220 (1979).
- Komiyama, N. H., Shih, D. T., Looker, D., Tame, J. & Nagai, K. Was the loss of the D helix in α globin a functionally neutral mutation? *Nature* **352**, 349–351 (1991).
- Perutz, M. F. Stereochemistry of cooperative effects in haemoglobin. *Nature* **228**, 726–739 (1970).
- Perutz, M. F. Nature of haem-haem interaction. *Nature* **237**, 495–499 (1972).
- Vallone, B., Bellelli, A., Miele, A. E., Brunori, M. & Fermi, G. Probing the $\alpha_1\beta_2$ interface of human hemoglobin by mutagenesis. role of the FG-C contact regions. *J. Biol. Chem.* **271**, 12472–12480 (1996).
- Park, S. Y., Yokoyama, T., Shibayama, N., Shiro, Y. & Tame, J. R. H. 1.25 Å resolution crystal structures of human haemoglobin in the oxy, deoxy and carbonmonoxy forms. *J. Mol. Biol.* **360**, 690–701 (2006).
- Silva, M. M., Rogers, P. H. & Arnone, A. A third quaternary structure of human hemoglobin A at 1.7-Å resolution. *J. Biol. Chem.* **267**, 17248–17256 (1992).
- Whitaker, T. L. et al. The D-helix in myoglobin and in the beta subunit of hemoglobin is required for the retention of heme. *Biochemistry* **34**, 8221–8226 (1995).
- Liong, E. C., Dou, Y., Scott, E. E., Olson, J. S. & Phillips, G. N. Waterproofing the heme pocket. Role of proximal amino acid side chains in preventing heme loss from myoglobin. *J. Biol. Chem.* **276**, 9093–9100 (2001).
- Tame, J. R. H. & Vallone, B. The structures of deoxy human haemoglobin and the mutant Hb Tyr $\alpha 42 \rightarrow$ His at 120 K. *Acta Crystallogr. D. Biol. Crystallogr.* **56**, 805–811 (2000).
- Cooper, C. E. et al. Engineering tyrosine residues into hemoglobin enhances heme reduction, decreases oxidative stress and increases vascular retention of a hemoglobin based blood substitute. *Free Radic. Biol. Med.* **134**, 106–118 (2019).
- Allen, K. N. & Vázquez-Medina, J. P. Natural tolerance to ischemia and hypoxemia in diving mammals: a review. *Front Physiol.* **10**, 1199 (2019).
- Baudin, V. et al. Allosteric properties of haemoglobin $\beta 41$ (C7) Phe \rightarrow Tyr: a stable, low-oxygen-affinity variant synthesized in *Escherichia coli*. *Biochim. Biophys. Acta* **1159**, 223–226 (1992).
- Mueser, T. C., Rogers, P. H. & Arnone, A. Interface sliding as illustrated by the multiple quaternary structures of liganded hemoglobin. *Biochemistry* **39**, 15353–15364 (2000).
- Tame, J. R. H. What is the true structure of liganded haemoglobin? *Trends Biochem. Sci.* **24**, 372–377 (1999).
- Ren, Z. Reaction trajectory revealed by a joint analysis of protein data bank. *PLoS One* **8**, e77141 (2013).
- Perutz, M. F. Species adaptation in a protein molecule. *Mol. Biol. Evol.* **1**, 1–28 (1983).
- Campbell, K. L. et al. Substitutions in woolly mammoth hemoglobin confer biochemical properties adaptive for cold tolerance. *Nat. Genet.* **42**, 536–540 (2010).
- Noguchi, H. et al. Structures of haemoglobin from woolly mammoth in liganded and unliganded states. *Acta Crystallogr. D. Biol. Crystallogr.* **68**, 1441–1449 (2012).
- Yuan, Y. et al. A biochemical-biophysical study of hemoglobins from woolly mammoth, Asian elephant, and humans. *Biochemistry* **50**, 7350–7360 (2011).
- Jessen, T. H., Weber, R. E., Fermi, G., Tame, J. & Braunitzer, G. Adaptation of bird hemoglobins to high altitudes: demonstration of molecular mechanism by protein engineering. *Proc. Natl. Acad. Sci. USA* **88**, 6519–6522 (1991).
- Weber, R. E., Jessen, T. H., Malte, H. & Tame, J. Mutant hemoglobins (α 119-Ala and β 55-Ser): functions related to high-altitude respiration in geese. *J. Appl. Physiol.* **75**, 2646–2655 (1993).
- Natarajan, C. et al. Convergent evolution of hemoglobin function in high-altitude andean waterfowl involves limited parallelism at the molecular sequence level. *PLoS Genet.* **11**, e1005681 (2015).

45. Natarajan, C. et al. Molecular basis of hemoglobin adaptation in the high-flying bar-headed goose. *PLoS Genet.* **14**, e1007331 (2018).
46. Berenbrink, M., Koldkjaer, P., Kepp, O. & Cossins, A. R. Evolution of oxygen secretion in fishes and the emergence of a complex physiological system. *Science* **307**, 1752–1757 (2005).
47. Yokoyama, T. et al. (2004) Novel mechanisms of pH sensitivity in tuna hemoglobin: a structural explanation of the Root effect. *J. Biol. Chem.* **279**, 28632–28640 (2004).
48. Mazzarella, L. et al. Minimal structural requirements for Root effect: crystal structure of the cathodic hemoglobin isolated from the Antarctic fish *Trematomus newnesi*. *Proteins* **62**, 316–321 (2006).
49. Ronda, L. et al. Role of tertiary structures on the Root effect in fish hemoglobins. *Biochim. Biophys. Acta* **1834**, 1885–1893 (2013).
50. Meir, J. U. & Ponganis, P. J. High-affinity hemoglobin and blood oxygen saturation in diving emperor penguins. *J. Exp. Biol.* **212**, 3330–3338 (2009).
51. Bautista, N. M., Damsgaard, C., Fago, A. & Wang, T. Carbon dioxide and bicarbonate accumulation in caiman erythrocytes during diving. *J. Exp. Biol.* **224**, jeb242435 (2021).
52. Weber, R. E. & White, F. N. Oxygen binding in alligator blood related to temperature, diving, and “alkaline tide”. *Am. J. Physiol.* **251**, R901–R908 (1986).
53. Storz, J. F., Opazo, J. C. & Hoffmann, F. G. Gene duplication, genome duplication, and the functional diversification of vertebrate globins. *Mol. Phylogenet. Evol.* **66**, 469–478 (2013).
54. Bautista, N. M. et al. Changes in hemoglobin function and isoform expression during embryonic development in the American alligator, *Alligator mississippiensis*. *Am. J. Physiol. Regul. Integr. Comp. Physiol.* **321**, R869–R878 (2021).
55. Komiya, N., Tame, J. & Nagai, K. A hemoglobin-based blood substitute: transplanting a novel allosteric effect of crocodile Hb. *Biol. Chem.* **377**, 543–548 (1996).
56. Geers, C. & Gros, G. Carbon dioxide transport and carbonic anhydrase in blood and muscle. *Physiol. Rev.* **80**, 681–715 (2000).
57. Locatelli, F. et al. Autologous gene therapy for hemoglobinopathies: from bench to patient’s bedside. *Mol. Ther.* **32**, 1202–1218 (2024).
58. Punjani, A., Rubinstein, J. L., Fleet, D. J. & Brubaker, M. A. cryoSPARC: algorithms for rapid unsupervised cryo-EM structure determination. *Nat. Methods* **14**, 290–296 (2017).
59. Akdel, M. et al. A structural biology community assessment of AlphaFold2 applications. *Nat. Struct. Mol. Biol.* **29**, 1056–1067 (2022).
60. Pettersen, E. F. et al. UCSF chimeraX: structure visualization for researchers, educators, and developers. *Protein Sci.* **30**, 70–82 (2021).
61. Emsley, P. & Cowtan, K. Coot: model-building tools for molecular graphics. *Acta Crystallogr. D: Struct.* **60**, 2126–2132 (2004).
62. Croll, T. ISOLDE: a physically realistic environment for model building into low-resolution electron-density maps. *Acta Crystallogr. D: Struct.* **74**, 519–530 (2018).
63. Yamashita, K., Palmer, C. M., Burnley, T. & Murshudov, G. N. Cryo-EM single-particle structure refinement and map calculation using *Servalcat*. *Acta Crystallogr. D: Struct.* **77**, 1282–1291 (2021).
64. Arnone, A. X-ray diffraction study of binding of 2,3-diphosphoglycerate to human deoxyhaemoglobin. *Nature* **237**, 146–149 (1972).
65. Richard, V., Dodson, G. G. & Mauguén, Y. Human deoxyhaemoglobin-2,3-diphosphoglycerate complex low-salt structure at 2.5 Å resolution. *J. Mol. Biol.* **233**, 270–274 (1993).

Acknowledgements

This paper is dedicated to our friend and mentor the late Kiyoshi Nagai FRS, who touched many lives with his personal warmth and transformative science. We thank Professors A. Tsuneshige and D. Crossley for their kind gifts of purified human HbA and alligator blood, respectively. K.T. acknowledges a JST university fellowship, grant number JPMJFS2140, Sasakawa Scientific Research Grant from The Japan Science Society, and SUNBOR scholarship. J.F.S. acknowledges grants from the NIH (R01HL087216) and NSF (OIA-1736249). Y.L. acknowledges a grant from JSPS (JP24H02264). T.N. acknowledges grants from JSPS (JP20H03216, JP23H02439, and JP24H02264). A.K. and G.K. acknowledge grants from JSPS (JP21H02417 and JP23H04958). A.F. acknowledges a NOVA grant from the Aarhus University Research Foundation (AUFF-E-2023-9-55). This research was partially supported by the Research Support Project for Life Science and Drug Discovery (Basis for Supporting Innovative Drug Discovery and Life Science Research (BINDS)) from AMED under Grant Number JP23ama121001. The cryo-EM experiments were performed at the RIKEN Yokohama cryo-EM facility and in part at the Institute for Protein Research, Osaka University.

Author contributions

K.T., Y.L., T.N. collected and processed EM data, and refined models. A.F., N.M.B., and J.F.S. purified samples, A.K. and G.K. prepared deoxy samples. K.T., Y.L., T.N., and J.R.H.T. analysed the models. J.R.H.T. wrote the draft manuscript, which was modified with the input of all authors.

Competing interests

The authors declare no competing interests.

Additional information

Supplementary information The online version contains supplementary material available at <https://doi.org/10.1038/s41467-024-49947-x>.

Correspondence and requests for materials should be addressed to Tomohiro Nishizawa or Jeremy R. H. Tame.

Peer review information *Nature Communications* thanks the anonymous reviewers for their contribution to the peer review of this work. A peer review file is available.

Reprints and permissions information is available at <http://www.nature.com/reprints>

Publisher’s note Springer Nature remains neutral with regard to jurisdictional claims in published maps and institutional affiliations.

Open Access This article is licensed under a Creative Commons Attribution 4.0 International License, which permits use, sharing, adaptation, distribution and reproduction in any medium or format, as long as you give appropriate credit to the original author(s) and the source, provide a link to the Creative Commons licence, and indicate if changes were made. The images or other third party material in this article are included in the article’s Creative Commons licence, unless indicated otherwise in a credit line to the material. If material is not included in the article’s Creative Commons licence and your intended use is not permitted by statutory regulation or exceeds the permitted use, you will need to obtain permission directly from the copyright holder. To view a copy of this licence, visit <http://creativecommons.org/licenses/by/4.0/>.

© The Author(s) 2024

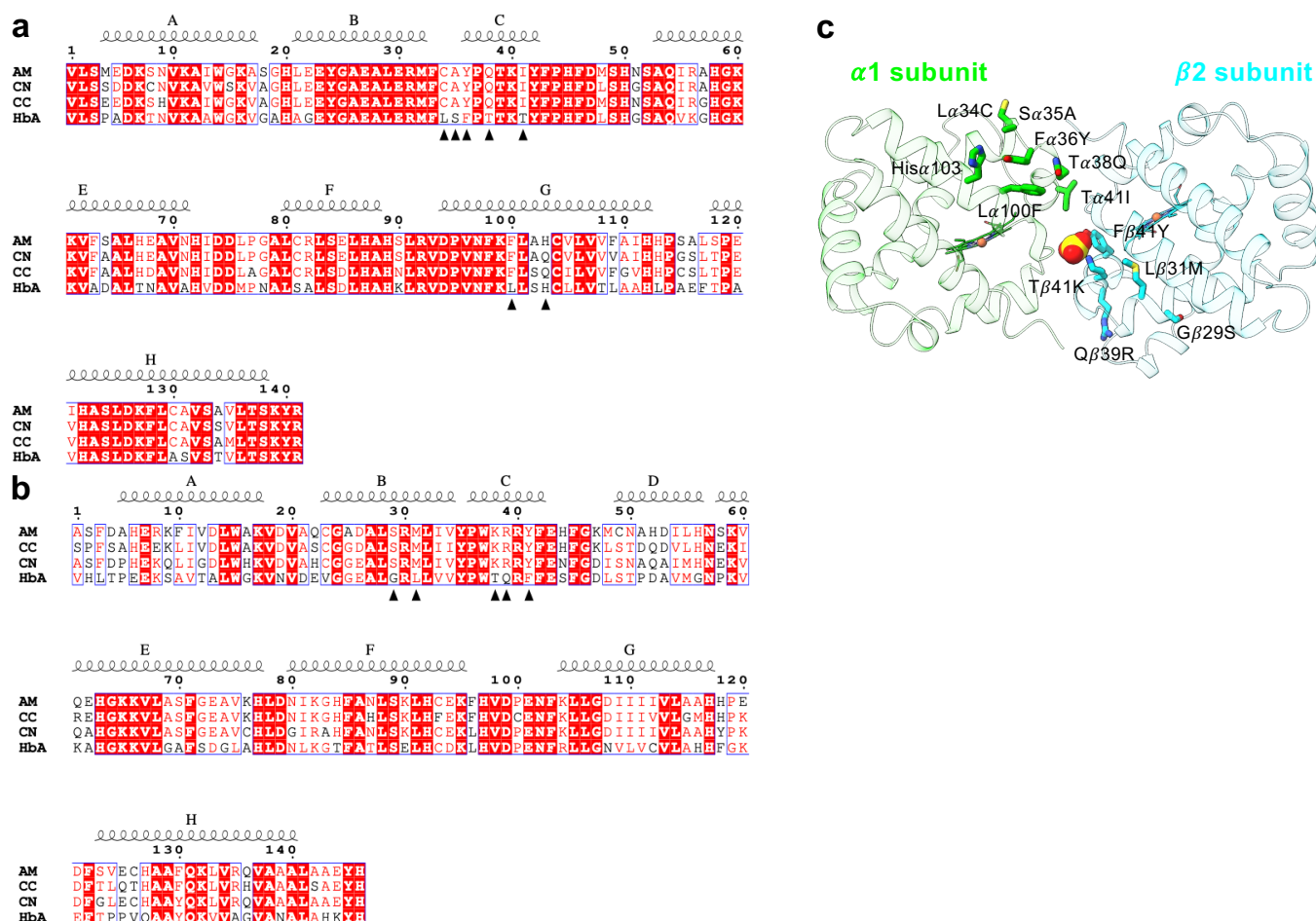


Figure S1. Sequence comparison of human and crocodilian Hb. (a) Alignment of human α globin with the homologous protein from three crocodilian species: AM (*Alligator mississippiensis*), CN (*Crocodylus niloticus*), and CC (*Caiman crocodilus*). Amino acid residues in common are shown in white on red; conservative mutations are shown in red. The traditional naming scheme of helical regions is shown above the sequences. Black triangles indicate residues mutated to create Hb Scuba. (b) Alignment of β globin sequences. These figures were made with ESPRIPT¹. (c) Residues mutated to create Hb Scuba are shown as sticks in a ribbon model of deoxy HbAM, showing the $\alpha_1\beta_2$ subunits. His α 103 is the only residue common to human HbA and HbAM at these 12 positions. The α_1 subunit is shown in lime and the β_2 subunit in cyan. The bicarbonate ion is shown as a CPK model, with carbon yellow and oxygen red.

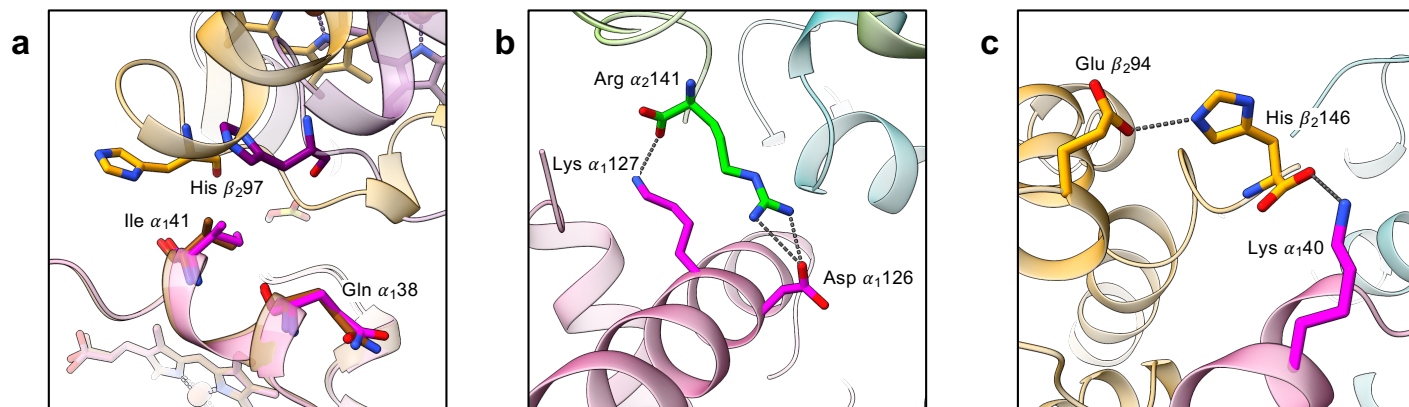


Figure S2. Conserved features of HbAM. (a) The movement of His β_297 relative to the α_1 C helix. The carbon atoms of the α_1 subunit are shown in magenta, of the α_2 subunit in cyan, of the β_1 subunit in lime, and of the β_2 subunit in orange. (b) Asp α_126 and Arg α_2141 . (c) Lys α_140 , His β_2146 and Glu β_294 .

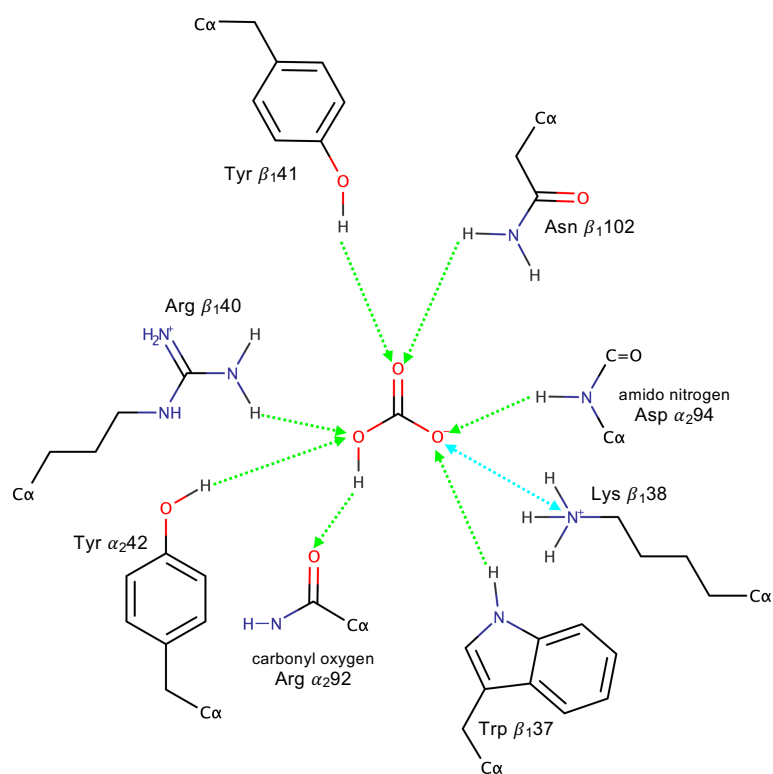


Figure S3. Schematic diagram of the bicarbonate binding site. Hydrogen bonds are shown as lime colored arrows, and a salt-bridge is shown as a two-headed arrow colored cyan. The carbonyl oxygen of Arg α 92 accepts a hydrogen bond from the bicarbonate ion.

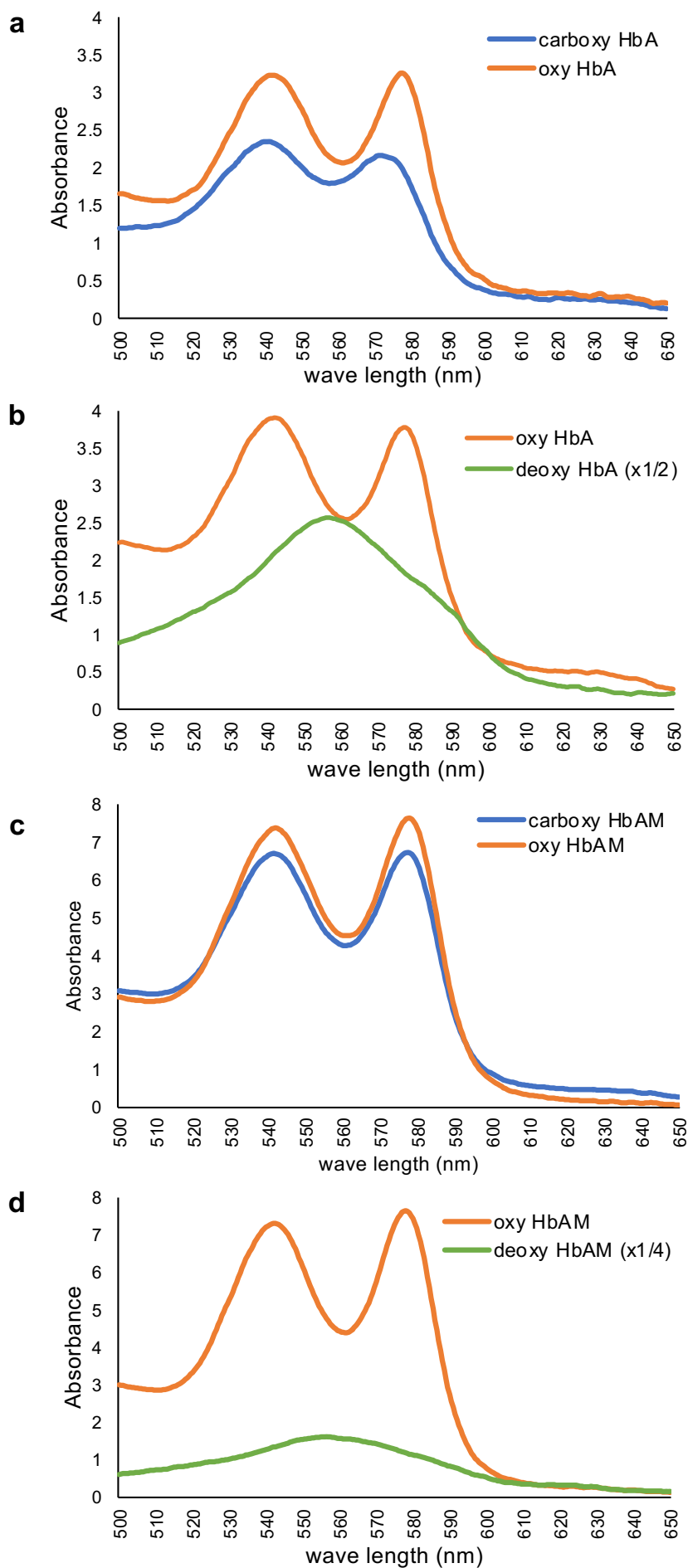


Figure S4. Visible spectra of the proteins. (a) Carbonmonoxy (blue) and oxy (orange) human HbA, measured under air before vitrification. **(b)** Oxy human HbA measured under oxygen-free nitrogen in the anaerobic chamber, before (orange) and after (green) addition of dithionite. **(c)** carbonmonoxy and oxy HbAM. **(d)** Oxy HbAM, measured in the anaerobic chamber before (orange) and after (green) addition of dithionite.

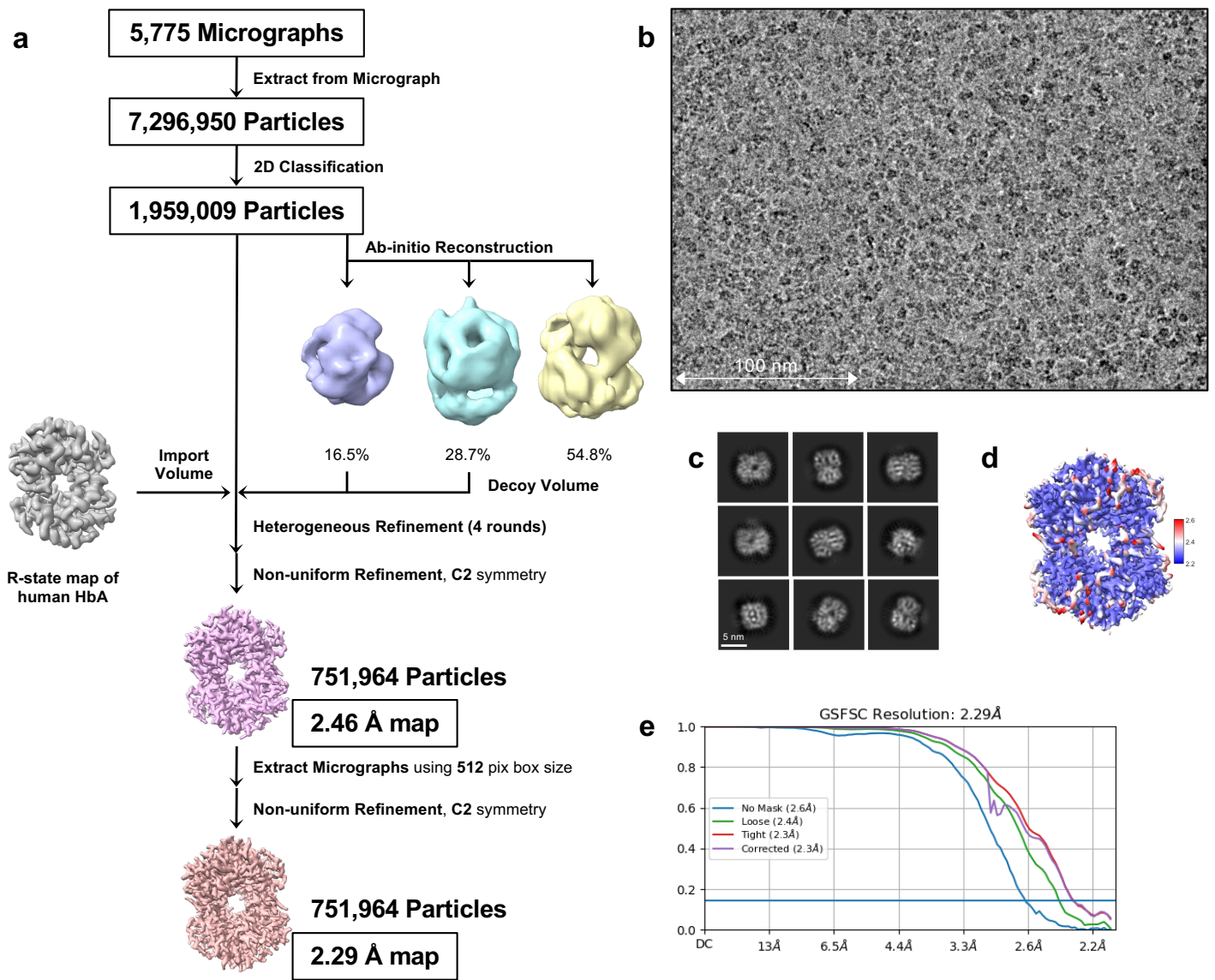


Figure S5. Structural analysis of carbonmonoxy HbAM. (a) Data processing workflow. (b) Representative cryo-EM micrograph. (c) Representative 2D class averages. (d) Local resolution estimation of the final map. (e) Gold-standard Fourier shell correlation plot.

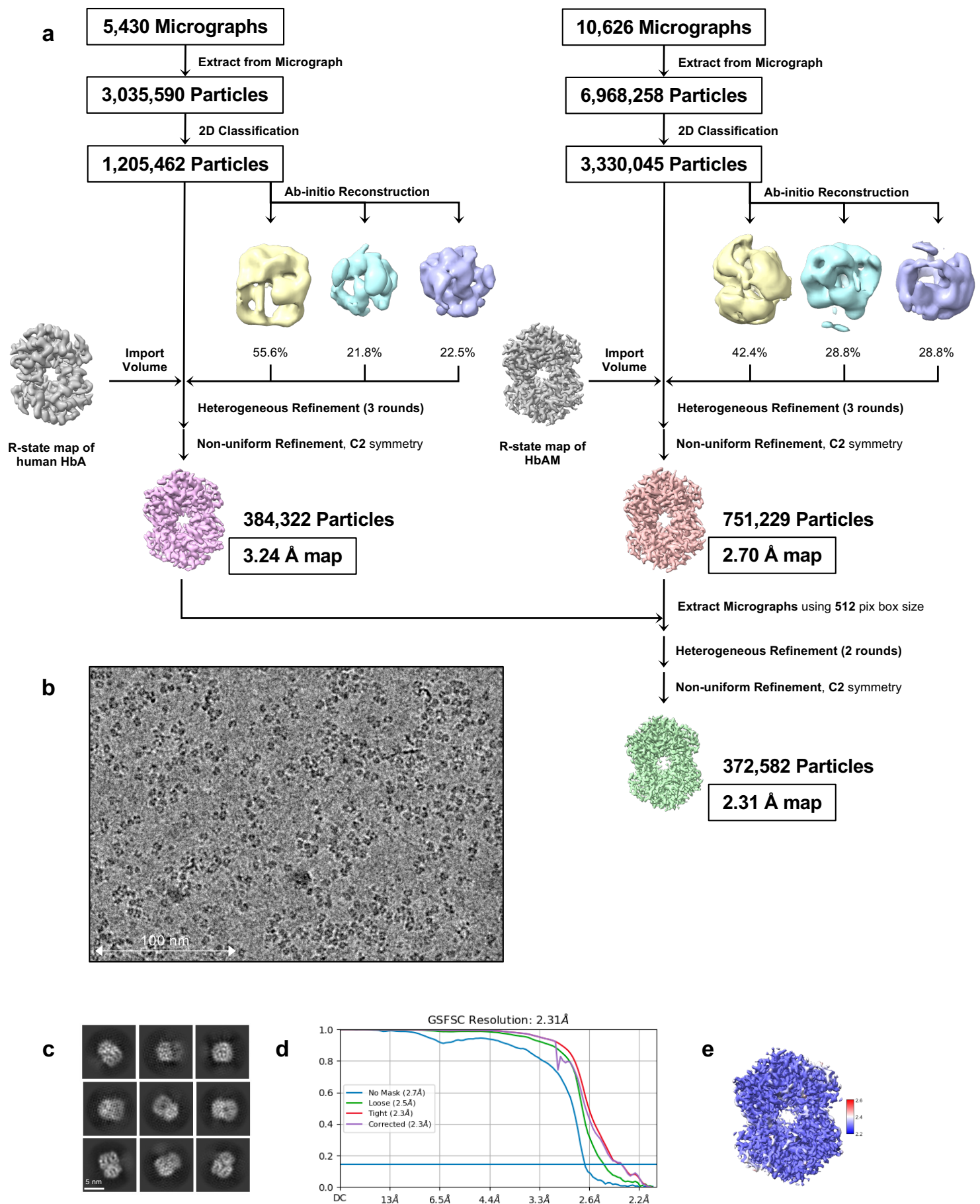


Figure S6. Structural analysis of oxy HbAM. (a) Data processing workflow. (b) Representative cryo-EM micrograph. (c) Representative 2D class averages. (d) Gold-standard Fourier shell correlation plot. (e) Local resolution estimation of the final map.

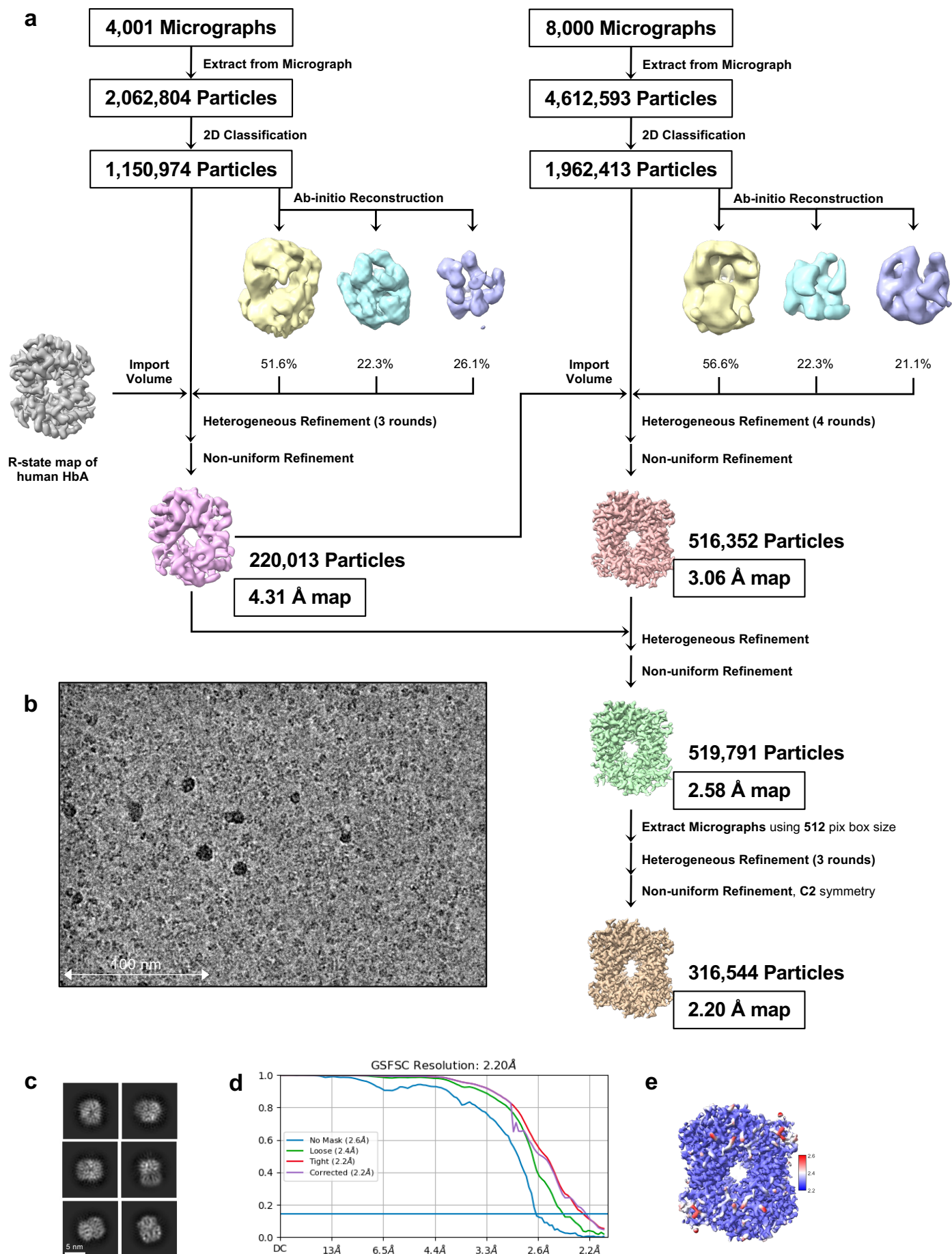


Figure S7: Structural analysis of deoxy HbAM. (a) Data processing workflow. (b) Representative cryo-EM micrograph. (c) Representative 2D class averages. (d) Gold-standard Fourier shell correlation plot. (e) Local resolution estimation of the final map.

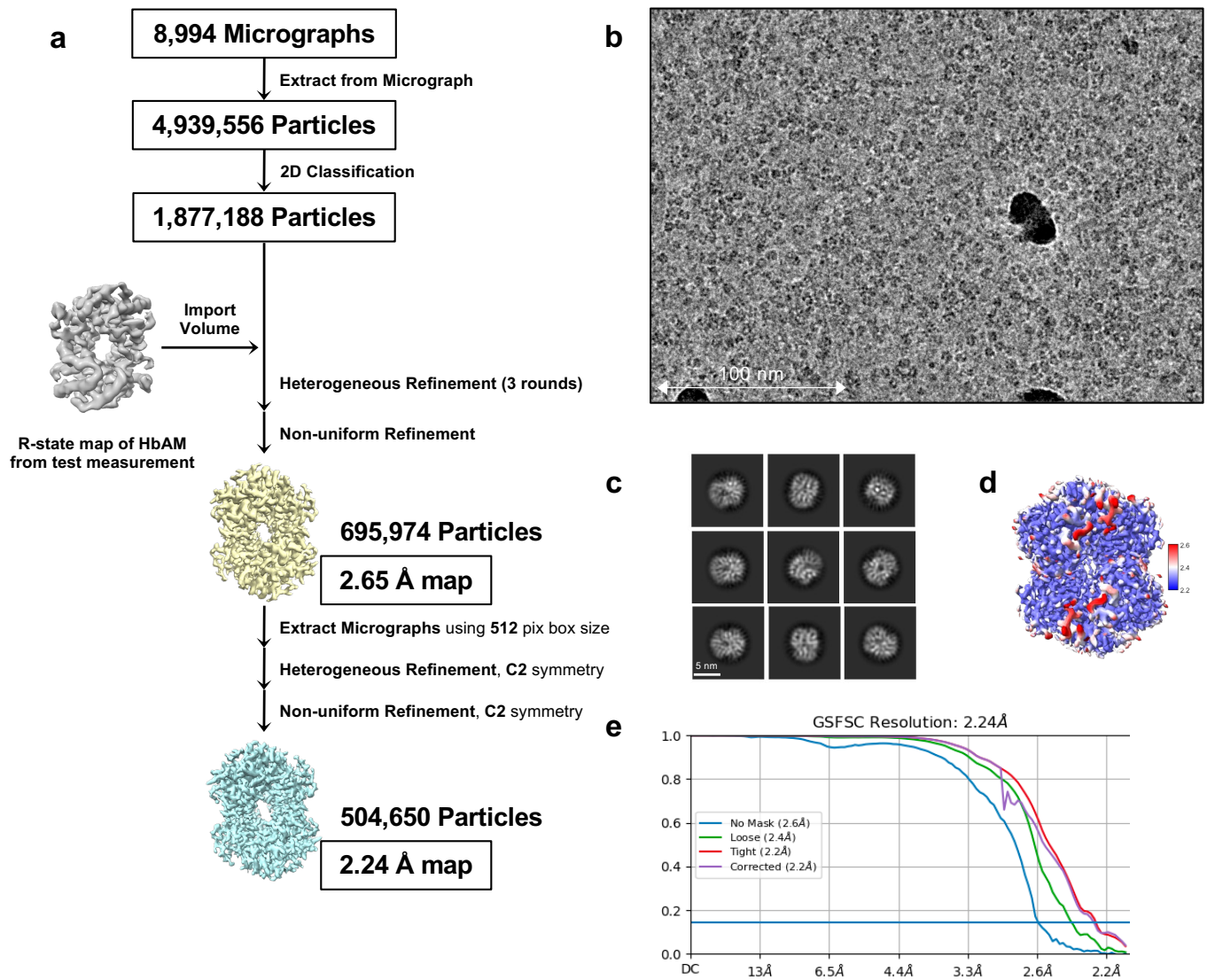


Figure S8. Structural analysis of carbonmonoxy human HbA. (a) Data processing workflow. (b) Representative cryo-EM micrograph. (c) Representative 2D class averages. (d) Local resolution estimation of the final map. (e) Gold-standard Fourier shell correlation plot.

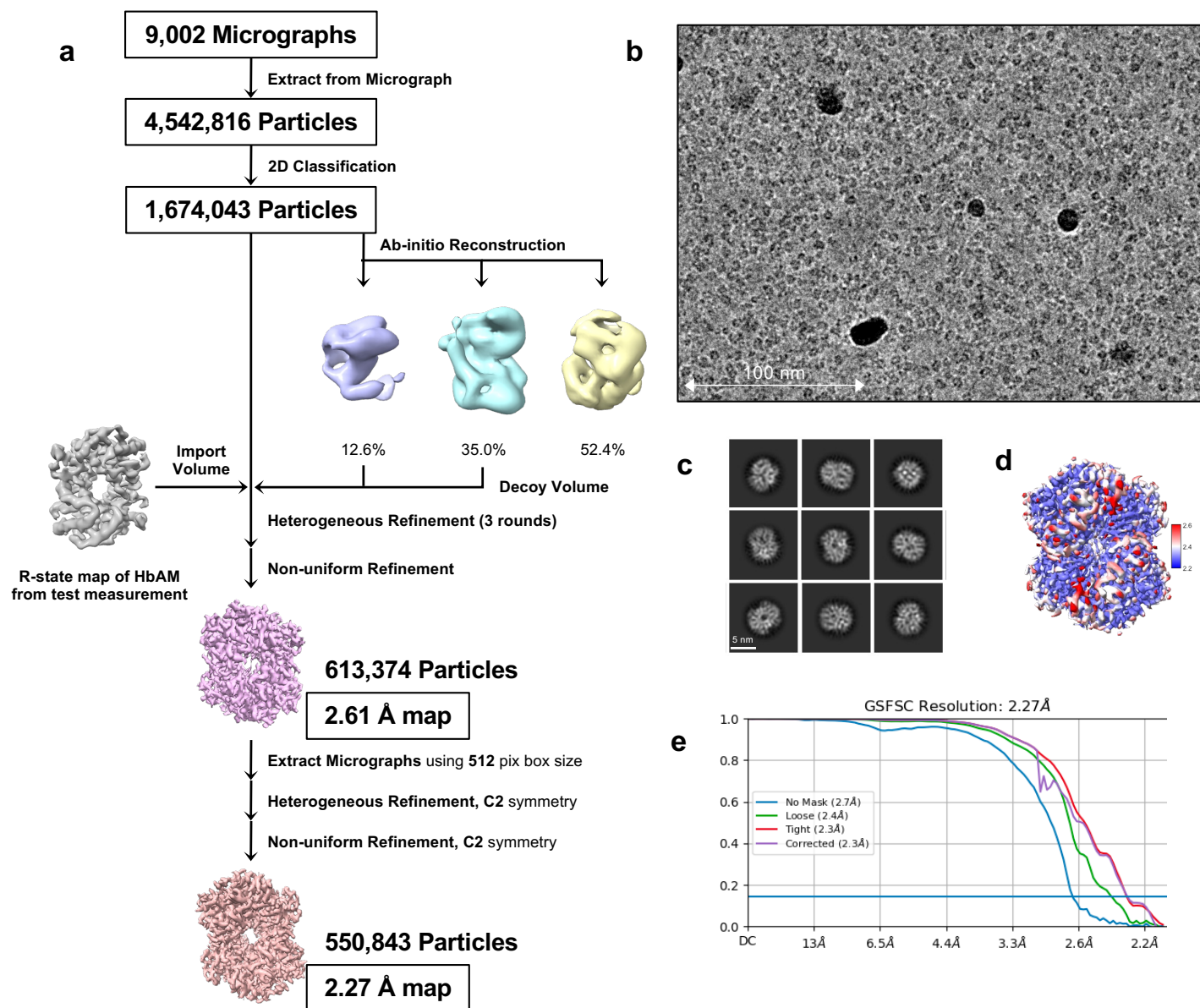


Figure S9. Structural analysis of oxy human HbA. (a) Data processing workflow. (b) Representative cryo-EM micrograph. (c) Representative 2D class averages. (d) Local resolution estimation of the final map. (e) Gold-standard Fourier shell correlation plot.

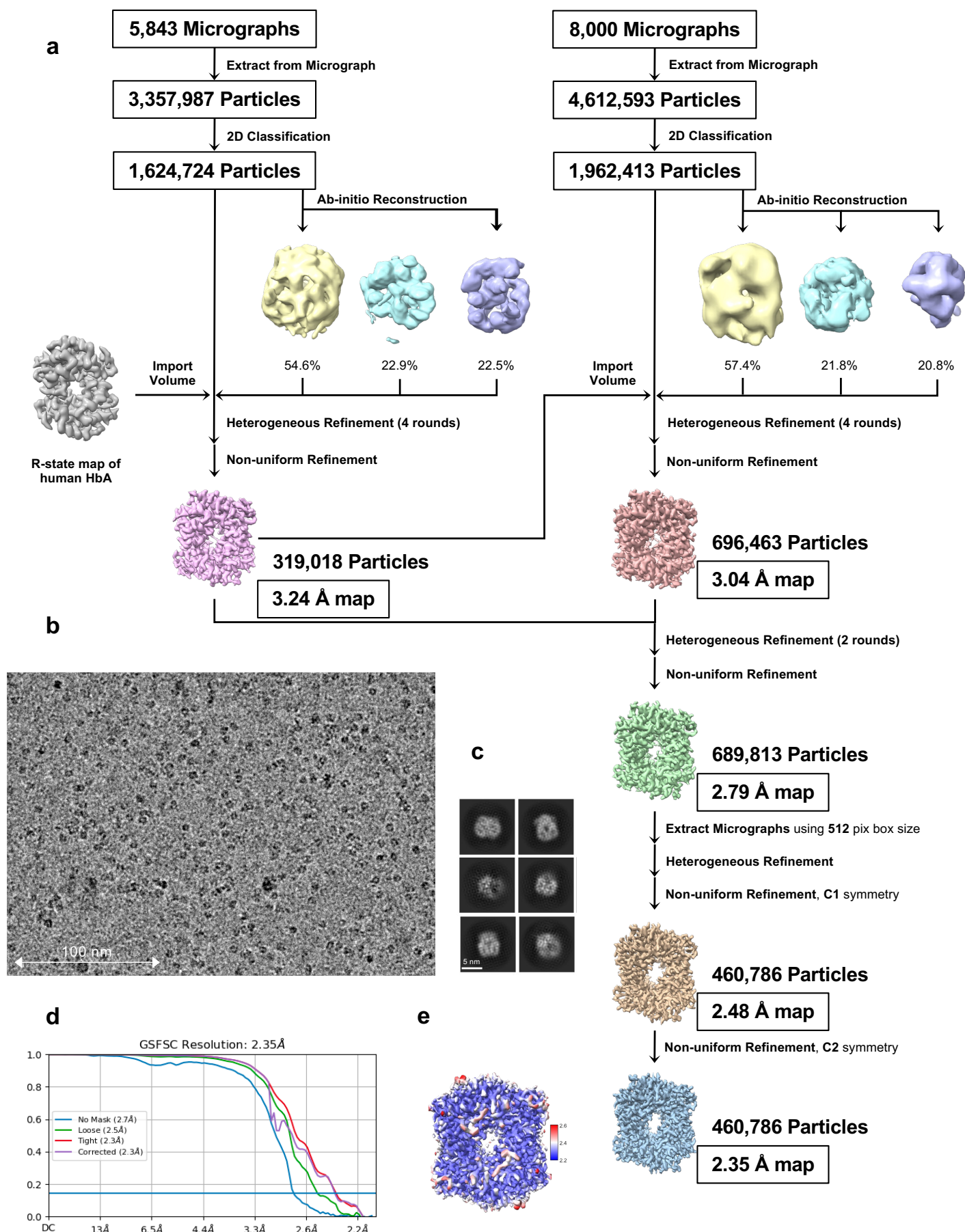


Figure S10. Structural analysis of deoxy human HbA. (a) Data processing workflow. (b) Representative cryo-EM micrograph. (c) Representative 2D class averages. (d) Gold-standard Fourier shell correlation plot. (e) Local resolution estimation of the final map.

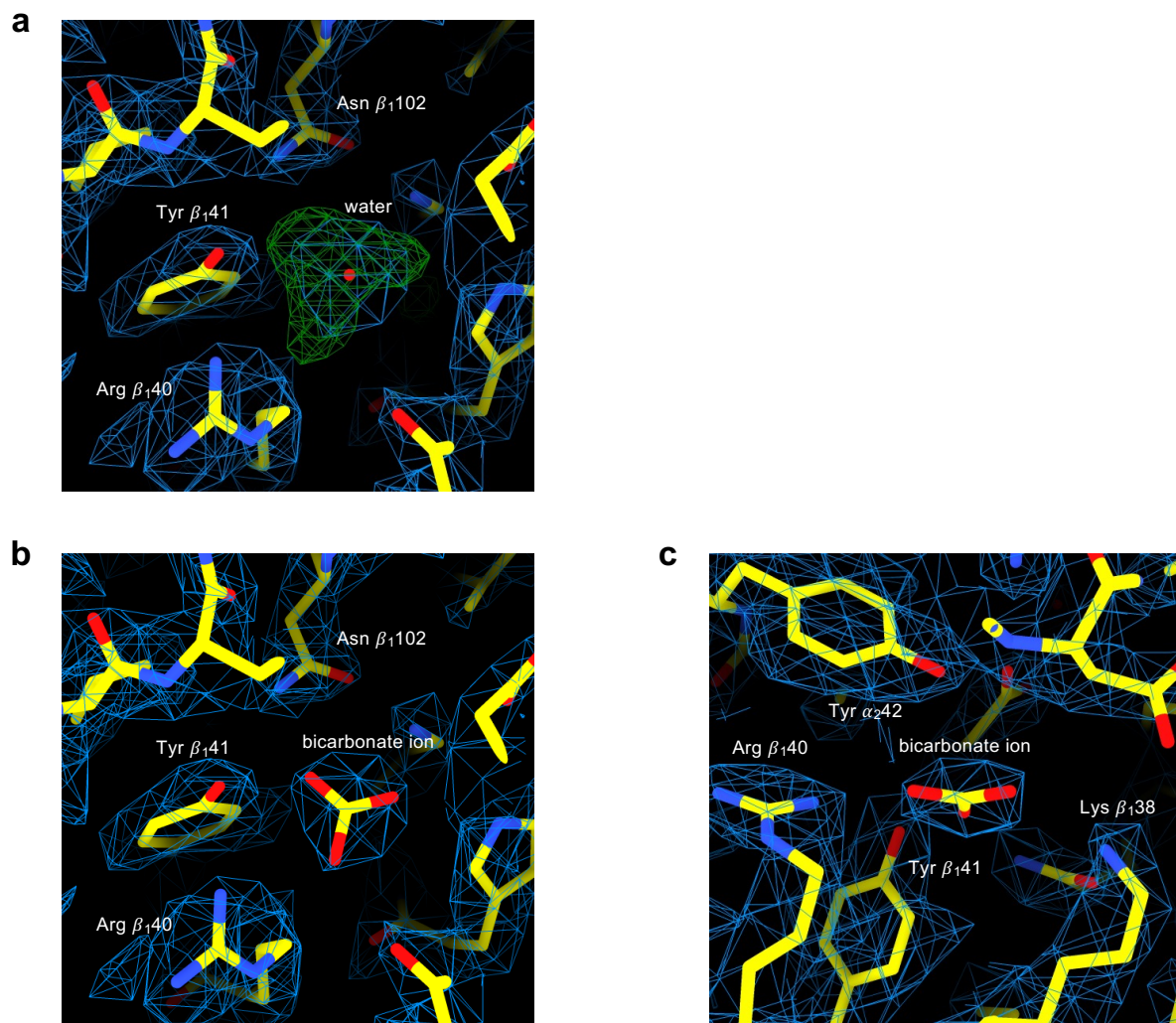


Figure S11. Density maps at the bicarbonate binding site. (a) The water molecule initially placed at this position (red sphere) is shown in the cryo-EM density map (blue) and the F_O-F_C positive map (green), which indicates a larger, non-spherical ligand. (b, c) The bicarbonate ion in the final model and the cryo-EM density map (blue) from two different angle.

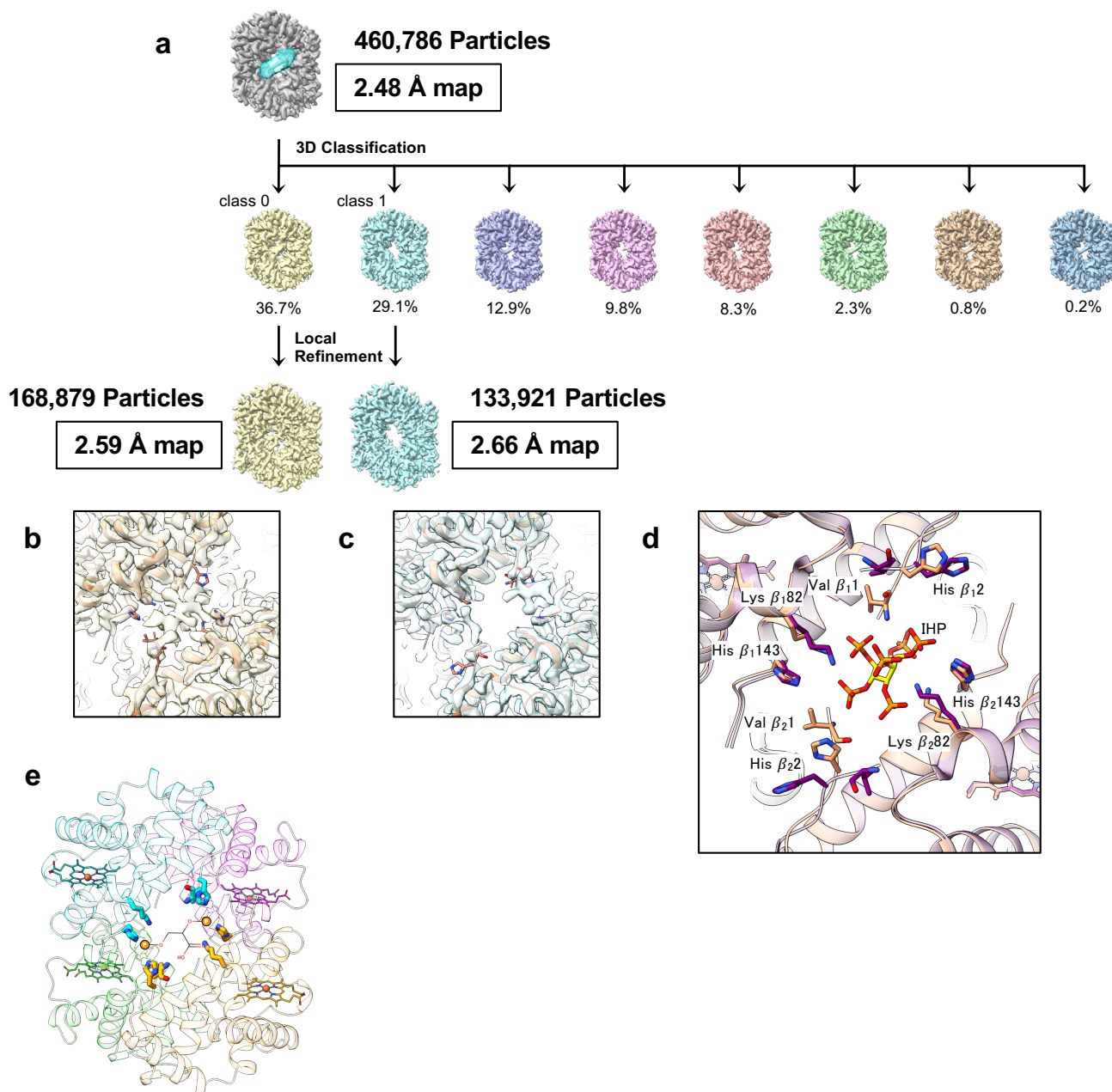


Figure S12. 3D classification of deoxy human HbA. (a) Workflow of 3D classification and local refinements. A mask around the IHP-like blob is shown in cyan. The particles were classified into eight classes (class 0-7, from left to right), and the maps of class 0 (yellow) and class 1 (light blue) were refined respectively. Close-up of the phosphate interacting site between two β subunits in the cryo-EM map of IHP-bound deoxy human HbA (b) and unliganded deoxy human HbA (c) generated from local refinement. (d) A possible conformation of IHP between the two β subunits of deoxy human HbA, superposed with carbonmonoxy human HbA. The carbon atoms of deoxy human HbA are colored salmon, those of carbonmonoxy human HbA are shown in purple, and those of IHP are shown in yellow. (e) A hypothetical model of the 2,3-DPG (diphosphoglycerate)-bound deoxy human HbA^{8,9}, with interacting side-chains shown as the sticks model. The carbon atoms of the α_1 subunit are shown in magenta, those of the β_1 subunit are shown in cyan, those of the α_2 subunit are shown in lime, and those of the β_2 subunit are shown in orange. 2,3-DPG is shown as the structural formula, and phosphate groups are shown as orange circles.

Table S1. Distances between atoms of ligands, heme, and histidines of the α subunit of carbonmonoxy human HbA and HbAM (**a**), and oxy human HbA and HbAM (**b**).

a

distance (Å)		2dn3	1bbb	CO-HbA	CO-HbAM	ideal
CO - C	HEM - Fe	1.74	1.77	1.88	1.98	1.75
CO - C	HEM - N α	2.72	2.83	2.69	2.78	
CO - O	His α 58 - N ϵ	3.30	3.23	3.02	2.57	
CO - C	His α 58 - N ϵ	3.44	3.47	2.91	2.72	
HEM - Fe	His α 87 - N ϵ	2.11	2.08	2.19	2.19	

b

distance (Å)		2dn1	O ₂ -HbA	O ₂ -HbAM	ideal
O ₂ - O _{near}	HEM - Fe	1.82	2.07	2.01	1.75
O ₂ - O _{near}	HEM - N α	2.71	3.03	2.97	
O ₂ - O _{near}	His α 58 - N ϵ	2.82	2.57	2.69	
O ₂ - O _{far}	His α 58 - N ϵ	2.70	2.95	2.85	
HEM - Fe	His α 87 - N ϵ	2.07	2.15	2.19	

Table S2. Interaction distances of the principal allosteric contacts of carbonmonoxy human HbA and HbAM (**a**), and deoxy human HbA and HbAM (**b**).

a					
distance (Å)		2dn3	1bbb	CO-HbA	CO-HbAM
Asp α_1 94 - O δ	Trp β_2 37 - N ϵ	3.67	3.77	3.64	3.38
Asp α_1 94 - O δ	Asn β_2 102 - N δ	2.74	2.75	2.97	2.92
Trp β_1 37 - N ϵ	Asn β_1 102 - N δ	2.95	3.03	2.99	3.02

b				
distance (Å)		2dn2	Deoxy HbA	Deoxy HbAM
Lys α_1 40 - N ζ	His β_2 146 - O	2.83	3.00	2.72
Tyr α_1 42 - O η	Asp β_2 99 - O δ	2.51	3.02	2.52
Asp α_1 94 - O δ	Trp β_2 37 - N ϵ	2.85	2.98	3.42
Asp α_1 126 - O δ	Arg α_2 141 - N η_1	2.78	2.78	2.66
	Arg α_2 141 - N η_2	2.95	2.79	3.42
Lys α_1 127 - N ζ	Arg α_2 141 - O	2.77	3.68	2.66
Asp β_1 94 - O δ	His β_1 146 - N ϵ	2.60	3.09	2.79

Table S3 RMSD comparisons between X-ray and cryo-EM models of all states of human HbA and HbAM (a, b).

a	RMSD (Å)	2dn1	2dn3	1bbb	Oxy HbA	CO-HbA	Oxy HbAM
	Oxy HbA	2.14	1.44	0.61			
	Carbonmonoxy HbA	2.16	1.46	0.58	0.21		
	Oxy HbAM	1.26	1.18	1.74	1.47	1.47	
	Carbonmonoxy HbAM	1.23	1.15	1.75	1.46	1.47	0.15
b	RMSD (Å)	2dn2	Deoxy HbA				
	Deoxy HbA	0.44					
	Deoxy HbAM	0.99	0.84				

	angle (°)
<u>2dn2</u>	0
Deoxy human HbA	1.3
<u>Deoxy HbAM</u>	3.1
2dn1 (Oxy)	14.7
<u>Oxy HbAM</u>	15.0
<u>2dn3 (CO)</u>	15.0
<u>Carbonmonoxy HbAM</u>	16.4
Oxy human HbA	19.9
<u>Carbonmonoxy human HbA</u>	22.1
<u>1bbb</u>	23.8

Table S4. Concerted rotation angles with respect to 2dn2 (X-ray model of the T-state deoxy human HbA) of all state structures of human HbA and HbAM. The colours of the underlines on the left column match the colours of the aligned models in Figure 2.

Residue	Distance (Å)
Trp β 37 - N ϵ	3.32
Lys β 38* - N ζ	2.77
Arg β 40 - N η	2.94
Tyr β 41* - O η	2.36
Asn β 102 - N δ	2.98
Tyr α 42 - O η	3.34
Arg α 92 - O _{carbonyl}	2.68
Asp α 94 - N _{amido}	3.44

Table S5. Interaction distances between bicarbonate ions and deoxy HbAM. The asterisks show the unique crocodilian residues directly binding bicarbonate.